# New Noncentered Icosahedral Nickel−Bismuth Carbonyl Clusters: Geometric Analysis of the Homologous $[Ni_{10}(EMe)_2(CO)_{18}]^{2-}$ Dianions (E = P, As, Sb, Bi) Containing Noncentered 1,12-$Ni_{10}E_2$ Icosahedral Cages[1]

Peter D. Mlynek and Lawrence F. Dahl*

*Department of Chemistry, University of Wisconsin−Madison, Madison, Wisconsin 53706*

*Received November 15, 1996*[⊗]

The designed reaction of $[Ni_6(CO)_{12}]^{2-}$ (**1**) with $MeBiCl_2$ in THF at low temperature (−78 °C) has given rise to the desired $[Ni_{10}(BiMe)_2(CO)_{18}]^{2-}$ dianion (**2**) as the major product (*ca.* 45% yield). This sought-after (methylbismuthinidene)nickel carbonyl cluster containing a noncentered 1,12-$Ni_{10}Bi_2$ icosahedral cage is the missing member of the known homologous $[Ni_{10}(EMe)_2(CO)_{18}]^{2-}$ series (E = P, As, Sb) whose members differ from one another only by the substitution of two bridging E atoms of the congeneric main-group V (15) elements into the two centrosymmetrically related (opposite) vertices of the icosahedral cage. The formulation of **2** in the $[NMe_4]^+$ salt was established unambiguously from X-ray crystallography and ascertained from a complete elemental analysis. This air-sensitive brown compound was also characterized by IR, cyclic voltammetry, negative-ion ESI mass spectrometry, and low-temperature $^{13}C\{^1H\}$ and $^1H$ NMR spectroscopy. The $[NMe_4]^+$ salt of the ethylbismuthinidene $[Ni_{10}(BiEt)_2(CO)_{18}]^{2-}$ (**3**) was similarly prepared, isolated, and structurally determined via a single-crystal X-ray diffraction study. Solid-state magnetic susceptibility measurements conclusively showed **2** (in the $[NMe_4]^+$ salt) to be diamagnetic at room temperature in accordance with it (and the other homologous members) being electronically equivalent (isolobal) with the classic regular icosahedral $[B_{12}H_{12}]^{2-}$ dianion in likewise possessing 13 skeletal electron pairs. A detailed comparison of the essentially identical molecular parameters of **2** and **3** with those of the three other isostructural $[Ni_{10}(EMe)_2(CO)_{18}]^{2-}$ clusters (E = P, As, Sb) provides illuminating information regarding particular geometric changes in the empty icosahedral 1,12-$Ni_{10}E_2$ cages arising from a systematic size variation in the two E atoms of the four congeneric group V (15) elements. Moreover, a comparative analysis of the molecular parameters of **2** with those of the previously reported $[Ni_{11}Bi_2(CO)_{18}]^{3-}$ trianion (**4**), which contains a Ni-centered (filled) 1,-12-$Ni_{10}Bi_2$ icosahedral cage, reveals marked geometric distortions upon the formal insertion of a centered (interior) Ni(*i*) into the icosahedral cage. Variable-temperature $^{13}C\{^1H\}$ NMR spectra of **2** in acetone-$d_6$ show fast terminal-bridge carbonyl exchange of the 18 COs at room temperature but limiting slow exchange at low temperature (−60 °C), as was also found for $[Ni_{10}(EMe)_2(CO)_{18}]^{2-}$ (E = P, Sb) previously.

## Introduction

Over the past 10 years there has been much progress made in transition-metal cluster chemistry, especially in the preparation and physicochemical characterization of high-nuclearity metal carbonyl clusters. One particularly active area in our laboratories has involved the preparation and physical/chemical characterization of close-packed nickel carbonyl clusters including ones with bridging main-group IV (14), V (15), or VI (16) atoms as well as giant-sized bimetallic nickel clusters with rhodium,[2] palladium,[3] gold,[4] and copper.[5]

The general synthetic route that has given rise to an astonishing array of large nickel/main-group carbonyl clusters has involved reactions of the $[Ni_6(CO)_{12}]^{2-}$ dianion (**1**)[6] with monomeric main-group reagents. Products isolated and structurally analyzed from X-ray crystallographic studies include ones with $Ni_xE_y$ cores, where E denotes main-group bridging atoms such as indium,[7] germanium,[8,9] tin,[10] phosphorus,[11−14] arsenic,[15]

* To whom correspondence should be addressed. E-mail: dahl@chem.wisc.edu. Fax: +608-262-0381.

⊗ Abstract published in *Advance ACS Abstracts,* March 15, 1997.

(1) (a) Presented in part at the 208th National Meeting of the American Chemical Society, Washington, DC, Aug 24, 1994. See: Mlynek, P. D.; Dahl, L. F. *Abstracts of Papers*; National Meeting of the Americal Chemical Society; American Chemical Society: Washington, DC, 1994; INOR 561. (b) Based in part on the Ph.D. thesis of P.D.M. at the University of Wisconsin−Madison, 1996.

(2) Nagaki, D. A.; Badding, J. V.; Stacy, A. M.; Dahl, L. F. *J. Am. Chem. Soc.* **1986**, *108*, 3825−3827.

(3) Kawano, M.; Bacon, J. W.; Campana, C. F.; Dahl, L. F. *J. Am. Chem. Soc.* **1996**, 7869−7870.

(4) (a) Whoolery, A. J.; Dahl, L. F. *J. Am. Chem. Soc.* **1991**, *113*, 6683−6685. (b) Whoolery Johnson, A. J.; Spencer, B.; Dahl, L. F. *Inorg. Chim. Acta* **1994**, *227*, 269−283.

(5) Mlynek, P. D. Ph.D. Thesis, University of Wisconsin−Madison, 1996.

(6) (a) Calabrese, J. C.; Dahl, L. F.; Cavalieri, A.; Chini, P.; Longoni, G.; Martinengo, S. *J. Am. Chem. Soc.* **1974**, *96*, 2616−2618. (b) Longoni, G.; Chini, P.; Cavalieri, A. *Inorg. Chem.* **1976**, *15*, 3025−3029.

(7) Demartin, F.; Iapalucci, M. C.; Longoni, G. *Inorg. Chem.* **1993**, *32*, 5536−5543.

(8) Ceriotti, A.; Demartin, F.; Heaton, B. T.; Ingallina, P.; Longoni, G.; Manassero, M.; Marchionna, M.; Masciocchi, N. *J. Chem. Soc., Chem. Commun.* **1989** 786−787.

(9) Zebrowski, J. P.; Hayashi, R. K.; Bjarnason, A.; Dahl, L. F. *J. Am. Chem. Soc.* **1992**, *114*, 3121−3123.

S0276-7333(96)00965-X CCC: $14.00 

antimony,[16−19] bismuth,[20] sulfur,[21] selenium,[22] or tellurium;[22] each of the main-group bridging atoms is either "bare" or ligated by alkyl or aryl substituents. Although these results indicate a rich diversity of large nickel carbonyl clusters with different main-group atoms, much experimental/theoretical work still needs to be carried out. In addition to the preparation of particular clusters in order to provide operational tests of structural/bonding hypotheses, reliable synthetic methodology must continue to be developed in order to obtain large metal clusters in sufficient quantities that their physical properties in both solid state and solution can be measured and their chemical reactivities explored.

Initial attempts in our laboratories eight years ago to obtain the *p*-tolylbismuthinidene $[Ni_{10}(BiR)_2(CO)_{18}]^{2-}$ dianion (R = *p*-$MeC_6H_4$) containing a noncentered 1,12-$Ni_{10}Bi_2$ icosahedral cage by reaction of the $[NMe_3Ph]^+$ salt of **1** with (*p*-tolyl)$BiBr_2$ in THF at −78 °C were unsuccessful; no carbonyl-containing Ni−Bi products were isolated.[16] On the basis of observed geometric trends in the known $[Ni_{10}(ER)_2(CO)_{18}]^{2-}$ dianions (R = Me[13] for E = P; R = Me[15] for E = As; R = Ph[16] for E = Sb) with empty icosahedral 1,12-$Ni_{10}E_2$ cages, it was then concluded that the intrapentagonal Ni−Ni′ distances, whose mean values uniformly increase by 0.1 Å from E = P to E = As and by 0.1 Å from E = As to E = Sb, would be too long for E = Bi to support reasonable intrapentagonal Ni−Ni′ bonding interactions. However, Longoni and co-workers[20] subsequently reported the synthesis of the $[Ni_{11}Bi_2(CO)_{18}]^{n-}$ anions ($n$ = 2, 3) as $[NEt_4]^+$ salts by reaction of **1** with $BiCl_3$ in THF at room temperature; the corresponding tetraanion ($n$ = 4) was also obtained in solution by chemical or electrochemical reduction of the di- or trianion. In addition to CV measurements that showed reversible electron-transfer behavior among the three anions ($n$ = 2−4), an X-ray crystallographic study of $[NEt_4]_3[Ni_{11}Bi_2(CO)_{18}]$ revealed that the trianion possesses a Ni-centered 1,12-$Ni_{10}Bi_2$ icosahedral cage that is geometrically analogous to the Ni-centered 1,12-$Ni_{10}Sb_2$ cage found in the $[Ni_{11}\{SbNi(CO)_3\}_2(CO)_{18}]^{n-}$ anions ($n$ = 2−4); these latter anions were previously reported by Longoni and co-workers[18] at the same time as our synthetic/structural results[16] on the related $[Ni_{10}(SbPh)_2(CO)_{18}]^{2-}$ dianion with the noncentered 1,12-$Ni_{10}Sb_2$ cage. The lack of residual basicity of the lone pair on each Bi atom in the $[Ni_{11}Bi_2(CO)_{18}]^{n-}$ ($n$ = 2−4) anions was evident by the tetraanion being oxidized to the dianion instead of either being protonated upon treatment with protonic acids or methylated upon reaction with methyl iodide.[20] In contrast, the closely related Ni-centered $[Ni_{11}\{SbNi(CO)_3\}_2(CO)_{18}]^{4-}$ tetraanion was found to react with MeI to give the Ni-centered $[Ni_{11}(SbMe)_2(CO)_{18}]^{2-}$; however, an attempt to remove the two Sb-attached $Ni(CO)_3$ substituents by reaction with CO was unsuccessful.[18]

The proven existence of the Ni-centered $[Ni_{11}Bi_2(CO)_{18}]^{n-}$ anions ($n$ = 2−4)[20] inspired us to design an appropriate synthetic route to prepare the missing bismuth member (**2**) of the aforementioned $[Ni_{10}(EMe)_2(CO)_{18}]^{2-}$ series (E = P,[13] As,[15] Sb[19]) for a comparative geometrical analysis with the other three members. Of particular interest was whether **2** could be prepared or whether the centered (interior) nickel atom was a necessary ingredient in order to stabilize the 1,12-$Ni_{10}Bi_2$ icosahedral cage. If successful, we also wanted to determine the salient geometrical differences between the desired $[Ni_{10}(BiMe)_2(CO)_{18}]^{2-}$ (**2**) and the crystallographically characterized $[Ni_{11}Bi_2(CO)_{18}]^{3-}$ trianion[20] in order to assess structural/bonding effects due to the formal insertion of the Ni-centered atom into the empty icosahedral $Ni_{10}Bi_2$ cage of **2**.

On the basis of the previous optimization of the synthetic procedure used in isolating the methylstibinidene $Ni_{10}Sb_2$ cluster,[19] a similar reaction led to the isolation of **2** as the major product. Analogous synthetic conditions also gave rise to the ethylbismuthinidene **3**. The results presented herein have fulfilled our goals. However, our repeated attempts to prepare the corresponding arylbismuthinidene $Ni_{10}Bi_2$ cluster were again unsuccessful.

## Results and Discussion

**Syntheses of Trialkylbismuth, Alkylbismuth Dihalide, and Dialkylbismuth Halide Monomers.** The trimethylbismuth intermediate was prepared *via* a modified procedure of that reported by Scherer *et al.*,[23] who in turn had altered the original Schäfer−Hein synthesis[24] of this compound. We observed that reactions of the methyl Grignard reagent with bismuth tribromide instead of bismuth trichloride gave better results in obtaining trimethylbismuth. In order to obtain $MeBiX_2$ (X = Cl, Br), metathesis of trimethylbismuth with 2 equiv of bismuth trihalide was found to work adequately; this procedure is similar to that used to obtain the $MeSbX_2$ analogues (X = Cl, Br).[25] When the reactant ratios were reversed, both dimethylbismuth chloride and bromide were produced in almost 100% yields. This synthetic pathway to dimethylbismuth bromide not only was found to be easier to perform but also gave a higher yield (54% vs 37%) than that obtained from an alternate route, developed by Marquardt,[26] involving the formation of dimethylbismuth bromide

(10) Zebrowski, J. P.; Hayashi, R. K.; Dahl, L. F. *J. Am. Chem. Soc.* **1993**, *115*, 1142−1144.
(11) (a) Lower, L. D.; Dahl, L. F. *J. Am. Chem. Soc.* **1976**, *98*, 5046−5047. (b) Arif, A. M.; Jones, R. A.; Schwab, S. T. *J. Coord. Chem.* **1987**, *16*, 51−57. (c) Rieck, D. F.; Rae, A. D.; Dahl, L. F. *J. Chem. Soc., Chem. Commun.* **1993**, 585−586. (d) Montag, R. A. Ph.D. Thesis, University of Wisconsin−Madison, 1982.
(12) Olmsted, N. M.; Power, P. P. *J. Am. Chem. Soc.* **1984**, *106*, 1495−1496.
(13) Rieck, D. F.; Gavney, J. A., Jr.; Norman, R. L.; Hayashi, R. K.; Dahl, L. F. *J. Am. Chem. Soc.* **1992**, *114*, 10369−10379.
(14) Gavney, J. A., Jr.; Hayashi, R. K.; Underiner, T. L.; Safford, L. K.; Roth, J. D.; Bjarnason, A.; Weaver, M. J.; Dahl, L. F. To be published.
(15) Rieck, D. F.; Montag, R. A.; McKechnie, T. S.; Dahl, L. F. *J. Am. Chem. Soc.* **1986**, *108*, 1330−1331.
(16) DesEnfants, R. E., II; Gavney, J. A., Jr.; Hayashi, R. K.; Rae, A. D.; Dahl, L. F.; Bjarnason, A. *J. Organomet. Chem.* **1990**, *383*, 543−572.
(17) Albano, V. G.; Demartin, F.; Iapalucci, M. C.; Longoni, G.; Sironi, A.; Zanotti, V. *J. Chem. Soc., Chem. Commun.* **1990**, 547−548.
(18) Albano, V. G.; Demartin, F.; Iapalucci, M. C.; Laschi, F.; Longoni, G.; Sironi, A.; Zanello, P. *J. Chem. Soc., Dalton Trans.* **1991**, 739−748.
(19) Mlynek, P. D.; Dahl, L. F. *Organometallics* **1997**, *16*, 1641.
(20) Albano, V. G.; Demartin, F.; Iapalucci, M. C.; Longoni, G.; Monari, M.; Zanello, P. *J. Chem. Soc., Dalton Trans.* **1992**, 497−502.
(21) Kahaian, A. J. Ph.D. Thesis, University of Wisconsin−Madison, 1992.
(22) Kahaian, A. J.; Thoden, J. B.; Dahl, L. F. *J. Chem. Soc., Chem. Commun.* **1992**, 353−355.
(23) Scherer, O. J.; Hornig, P.; Schmidt, M. *J. Organomet. Chem.* **1966**, *6*, 259−264.
(24) Schäfer, K.; Hein, F. *Z. Anorg. Allg. Chem.* **1917**, *100*, 297−302.
(25) Nunn, M.; Sowerby, D. B.; Wesolek, D. M. *J. Organomet. Chem.* **1983**, *251*, C45−C46.
(26) Marquardt, A. *Ber. Deut. Chem. Ges.* **1887**, *20*, 1516−1523.

from the spontaneous decomposition of trimethylbismuth dibromide which was synthesized by the bromination of trimethylbismuth.

Ethylbismuth dichloride was prepared in a similar manner to that of the methylbismuth dichloride; the only significant difference was that higher temperatures were needed to distill the triethylbismuth intermediate. As observed with other trialkylpnicogens, caution must also be used when handling the intermediate trialkylbismuth reagents.[27]

**Syntheses of the $[Ni_{10}(BiR)_2(CO)_{18}]^{2-}$ Dianions (R = Me (2), Et (3)).** The preparations of **2** and **3** were achieved by reactions of **1** with 2 equiv of the appropriate alkylbismuth dichloride at −78 °C in THF, followed by solvent removal and subsequent extractions. Similar preparations of the homologous phosphorus and arsenic members, $[Ni_{10}(ER)_2(CO)_{18}]^{2-}$ (E = P, As), also gave rise to other intriguing Ni−E carbonyl byproducts including the electronically equivalent (isolobal) $[Ni_9(ER)_3(CO)_{15}]^{2-}$ and $[Ni_8(ER)_4(CO)_{12}]^{2-}$ dianions (E = P,[13] As[15,28]) containing empty icosahedral 1,2,12-$Ni_9E_3$ and 1,2,9,12-$Ni_8E_4$ cages, respectively. On the other hand, aside from decomposition products, reaction of either the methyl- or ethylbismuthine reagent with **1** only produced the corresponding $[Ni_{10}(BiR)_2(CO)_{18}]^{2-}$ dianion (R = Me (**2**), Et (**3**)) with the empty 1,12-$Ni_{10}Bi_2$ icosahedral cage. Similarly, only the homologous $[Ni_{10}(SbR)_2(CO)_{18}]^{2-}$ dianions (R = Me, Et, $^i$Pr, $^t$Bu, Ph, *p*-$FC_6H_4$) were isolated from reactions of stibine reagents with **1**, in spite of considerable efforts[16,19] to detect the possible existence of the hypothetical $[Ni_9(SbR)_3(CO)_{15}]^{2-}$ and $[Ni_8(SbR)_4(CO)_{12}]^{2-}$ dianions.

In contrast to icosahedral clusters of the other congeneric group V (15) elements being obtained from reactions performed at room temperature, low-temperature reactions must be carried out in order to obtain **2** and **3**; at room temperature only black insoluble powders were isolated. Similar reactions attempted in acetonitrile at −40 °C also did not produce any CO-containing clusters.

Syntheses of the analogous $[Ni_{10}(SbR)_2(CO)_{18}]^{2-}$ dianions (R = alkyl, Ph) were accomplished by reactions of **1** with either $R_2SbX$ or $RSbX_2$.[16,19] However, we were not successful in obtaining any detectable quantities of **2** or **3** or any other Ni−Bi carbonyl cluster under similar conditions with either monoalkylbismuth dibromide or dialkylbismuth bromide or chloride reagents. It is possible that the light-sensitive dialkylbismuth chloride or bromide[29] decomposed preferentially to other unreactive products instead of reacting under our boundary conditions with **1**. Hence, the only known synthetic pathway (to date) in isolating **2** or **3** involves the reaction of the appropriate monoalkylbismuth dichloride with **1**.

It is necessary that the bismuth reagent has one attached alkyl group in order that each of the two bismuth atoms in the final $Ni_{10}Bi_2$ carbonyl cluster possess a one-electron-donating substituent; reactions by Longoni and co-workers[20] of bismuth trihalide with **1** gave rise to $[Ni_{11}Bi_2(CO)_{18}]^{n-}$ anions ($n$ = 2, 3) that contain a Ni-centered icosahedral $Ni_{10}Bi_2$ cage with a lone electron-pair on each Bi atom[20] instead of a possible Bi-attached one-electron-donating halogen substituent.

Another indicated requirement of this reaction is that the bismuth reagent contain a halide ligand. Our attempted reactions of several trialkylbismuth reagents with **1** under various conditions did not generate any nickel−bismuth carbonyl clusters. The apparent driving force behind the formation of nickel−E(15) carbonyl clusters from reactions of various monomeric E(15) reagents with **1** is the formation of nickel(II) halide as a decomposition byproduct.

Whereas reactions of aryl-containing phosphorus, arsenic, and antimony halide reagents with **1** have resulted in the formation of Ni−E carbonyl clusters (E = P, As, Sb) with E-attached aryl substituents, prior attempts[16] to prepare the analogous $Ni_{10}Bi_2$ carbonyl cluster with Bi-attached *p*-tolyl substituents and our recent attempts to synthesize the same hypothetical cluster with phenyl substituents both failed. Instead, reactions of 2 equiv of either (*p*-$MeC_6H_4$)$BiCl_2$ or Ph$BiCl_2$ with **1** in THF at low temperature (−78 °C) produced dark insoluble material and $Ni(CO)_4$. Noteworthy is that the mean bond dissociation energy of a Bi−R fragment (R = Me or Ph) is markedly smaller than that of the same Sb−R fragment (*i.e.*, in general, the mean bond dissociation energy, $\bar{D}$(E−R), decreases upon going from E = P to E = Bi).[30] Nonetheless, this inability to isolate an aryl-substituted $Ni_{10}Bi_2$ carbonyl cluster is perplexing in light of the fact that the mean bond dissociation energy for Bi−Me compounds is significantly less than that for Bi−Ph compounds.[30] One possible rationalization is that even though the Bi−Ph bond is stronger than a Bi−Me bond, it is still too weak in the hypothetical $[Ni_{10}(BiPh)_2(CO)_{18}]^{2-}$ dianion to overcome the energetic effects caused by increased steric crowding of the ligand polyhedron about the icosahedral 1,12-$Ni_{10}Bi_2$ cage.

**Structural/Bonding Features of $[Ni_{10}(BiR)_2(CO)_{18}]^{2-}$ Dianions (R = Me (2), Et (3)).** Each of these isostructural dianions, **2** and **3**, can be viewed as a pentagonal antiprism of 10 surface Ni(*s*) atoms that is capped on the upper and lower pentagonal faces by bismuth atoms (Figure 1b). The resulting $Ni_{10}Bi_2$ icosahedral cage in **2** and **3** is enveloped by essentially identical arrangements of the 2 Bi-attached alkyl substituents and 18 carbonyl ligands. Each dianion lies on a crystallographic inversion center such that one-half of the icosahedral cage corresponding to a Bi-capped nickel pentagon constitutes the crystallographically independent unit. Thus, of the 10 Ni(*s*)−E, 10 intrapentagonal Ni(*s*)−Ni(*s*′), and 10 interpentagonal Ni(*s*)−Ni(*s*′) edges in each icosahedral 1,12-$Ni_{10}Bi_2$ cage, only 5 edges of each kind are independent. As expected for an empty $Ni_{10}Bi_2$ cage, each dianion is greatly deformed from a regular spherical icosahedron of $I_h$ symmetry (as in $[B_{12}H_{12}]^{2-}$) by a large oblate compression along the pseudo-5-fold axis passing through Bi and Bi′. Although the average overall geometry of the empty icosahedral $Ni_{10}Bi_2$ cage conforms to $D_{5d}$ symmetry, inclusion of the 18 carbonyl ligands reduces the symmetry of both **2** and

(27) $Me_3Bi$ is a very active poison when contacted by inhalation, orally, or though the intact skin. For a review of pharmacology of trimethylbismuth, see: Sollmann, T.; Seifter, J. *J. Pharmacol.* **1939**, *67*, 17−49.

(28) Whoolery, A. J. Ph.D. Thesis, University of Wisconsin−Madison, 1993.

(29) Wieber, M.; Sauer, I. *Z. Naturforsch.* **1984**, *39b*, 887−889.

(30) (a) $\bar{D}$(Bi−Me) = 36 kcal/mol, $\bar{D}$(Bi−Ph) = 48 kcal/mol: Skinner, H. A.; Conner, J. A. *Pure Appl. Chem.* **1985**, *57*, 79−88. (b) $\bar{D}$(Bi−Me) for $BiMe_3$ = 34.1 ± 1.1 kcal/mol, $\bar{D}$(Bi−Ph) for $BiPh_3$ = 42.1 kcal/mol: Wieber, M. Bismuth-Organische Verbindungen. In *Gmelin Handbuch der Anorganischen Chemie*, 8th ed.; Springer-Verlag: Berlin, 1977; Vol. 47, pp 47, 68.

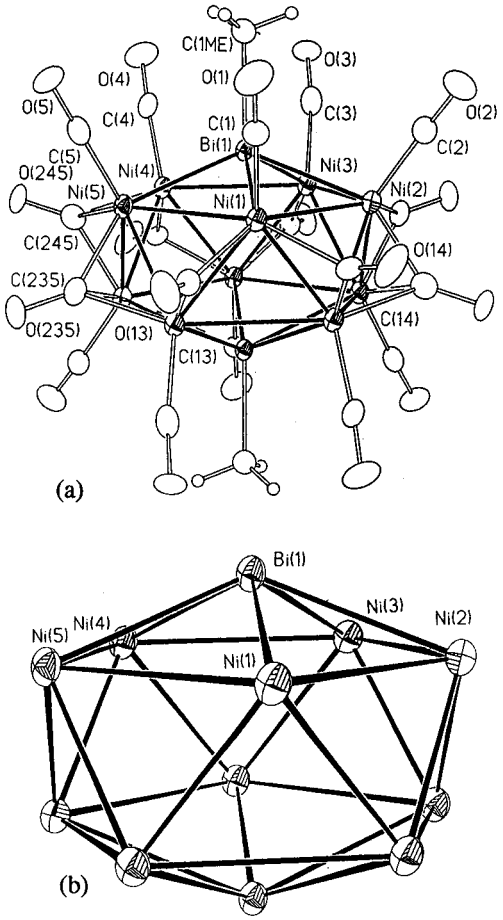


**Figure 1.** (a) Configuration of the $[Ni_{10}(BiMe)_2(CO)_{18}]^{2-}$ dianion (**2**) in the $[NMe_4]^+$ salt. This dianion, which possesses 10 terminal, 4 doubly bridging, and 4 triply bridging carbonyl ligands, has crystallographic $C_i$-$\bar{1}$ site symmetry and closely conforms to $C_{2h}$-2/*m* symmetry. The independent atoms are labeled. (b) Same view of the noncentered $Ni_{10}Bi_2$ cage of **2**. This empty cage may be envisioned as either a 1,12-disubstituted icosahedron or a pentagonal antiprism of 10 surface Ni(*s*) atoms that is capped on both pentagonal faces by bismuth atoms. Means of the five independent Ni(*s*)−Bi edges, five independent *intrapentagonal* Ni(*s*)−Ni(*s*′), and five independent *interpentagonal* Ni(*s*)−Ni(*s*′) edges are 2.63, 2.88, and 2.50 Å, respectively.

**3** from $D_{5d}$ to $C_{2h}$-2/*m*. Especially noteworthy is that the virtually identical dispositions of the 10 terminal and 4 doubly and 4 triply bridging COs under pseudo-$C_{2h}$ symmetry in both dianions produce analogous geometrical deformations of the 1,12-$Ni_{10}Bi_2$ cages.

Examination of corresponding independent individual distances between **2** and **3** in Tables 2 and 3, respectively, shows analogous large variations of one interpentagonal and two intrapentagonal Ni(*s*)−Ni(*s*′) distances from their mean values under assumed $D_{5d}$ symmetry. The two tables also show that the nonbonding Bi···Bi′ distance in **2** is significantly shorter by 0.07 Å than that in **3**; this somewhat larger oblate compression along the pseudo-5-fold Bi···Bi′ axis in **2** containing two smaller Bi-attached methyl substituents compared to **3** containing two Bi-attached ethyl substituents may be rationalized from steric effects of the ligand polyhedron involving nonbonding interactions of the two alkyl substituents with the closest carbonyl groups.

According to the polyhedral skeletal electron-pair (PSEP) model,[31] a *closo* deltahedron (*i.e.*, a completely closed triangulated polyhedron) should possess ($n$ + 1) electron pairs for skeletal cluster bonding. The 12-vertex icosahedral $Ni_{10}Bi_2$ cage should therefore have 13 skeletal electron pairs involved in globally delocalized bonding. The PSEP model assumes that only three internal valence orbitals at each vertex are involved in skeletal cluster bonding. An observed electron-pair count of 13 for each of the icosahedral $Ni_{10}Bi_2$ cages in **2** and **3** results from each Ni(CO), BiR, and CO donating zero, two, and one skeletal electron pairs, respectively, with the remaining skeletal electron pair being provided by the −2 charge of the dianion (*i.e.*, 10 × 0(NiCO) + 2 × 2(BiR) + 8 × 1(CO) + 1(charge) = 13). The other electronically equivalent (isolobal) members of the homologous $[Ni_{10}(ER)_2(CO)_{18}]^{2-}$ series (E = P, As, Sb, Bi) and the prototype $[B_{12}H_{12}]^{2-}$ dianion and its carborane derivatives likewise possess 13 skeletal electron pairs. For any of the $Ni_{10}(ER)_2$ members this number of electron pairs corresponds to the observed number of cluster valence electrons (CVEs) being 150 electrons (*i.e.*, 10 × 10(Ni) + 2 × 6(ER) + 18 × 2(CO) + 2(charge) = 150). This equivalence in electron counting arises because the skeletal electron-pair model assumes that each icosahedral vertex utilizes only 3 *internal* orbitals for metal cluster bonding; consequently, 12 valence electrons from the filled 6 *external* metal orbitals for each of the 10 Ni(CO) fragments and 2 valence electrons from the one filled *external* main-group E orbital for each of the 2 ER fragments must be subtracted from 150 CVEs. The resulting 26 skeletal valence electrons occupy 13 *internal* bonding MOs in accordance with the skeletal electron-pair count. Application of the different valence electron-counting models developed by Mingos,[32] by Teo and Zhang,[33] and by King[34] to any of the

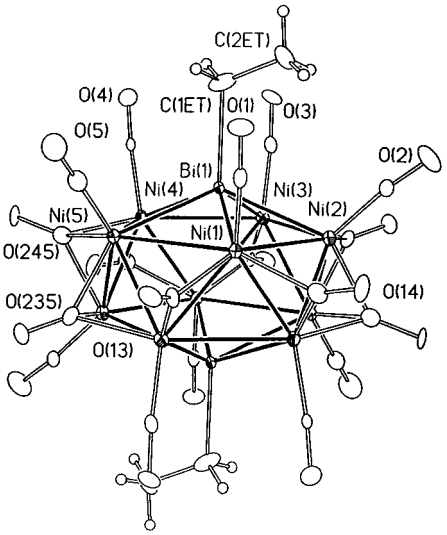


**Figure 2.** Configuration of the $[Ni_{10}(BiEt)_2(CO)_{18}]^{2-}$ dianion (**3**) in the $[NMe_4]^+$ salt.

(31) (a) Wade, K. *J. Chem. Soc., Chem. Commun.* **1971**, 792−793. (b) Wade, K. *Electron Deficient Compounds*; Thomas Nelson and Sons, Ltd.: London, 1971. (c) Wade, K. *Adv. Inorg. Chem. Radiochem.* **1976**, *18*, 1−66.

(32) Mingos, D. M. P.; Zhenyang, L. *J. Chem. Soc., Dalton Trans.* **1988**, 1657−1664 and references therein. (b) Mingos, D. M. P.; May, A. P. In *The Chemistry of Metal Cluster Complexes*; Shriver, D. F., Kaesz, H. D., Adams, R. D., Eds.; VCH Publishers: New York, 1990; Chapter 2, pp 11−119. (c) Mingos, D. M. P.; Wales, D. J. *Introduction to Cluster Chemistry*; Prentice Hall: Old Tappan, NJ, 1990.

(33) Teo, B. K.; Zhang, H.; Kean, Y.; Dang, H.; Shi, X. *J. Chem. Phys.* **1993**, *99*, 2929−2941. (b) Teo, B. K.; Longoni, G.; Chung, F. R. K. *Inorg. Chem.* **1984**, *23*, 1257−1266. (c) Teo, B. K. *Inorg. Chem.* **1985**, *24*, 1627−1638.

**Table 1. Crystal Data and Structural Refinement Parameters for the $[NMe_4]^+$ Salts of $[Ni_{10}(BiR)_2(CO)_{18}]^{2-}$ (R = Me (2), Et (3))**

| | | |
|---|---|---|
| **Crystal Data** | | |
| identification code | **2** | **3** |
| formula | $C_{28}H_{30}Bi_2N_2Ni_{10}O_{18}$ | $C_{30}H_{34}Bi_2N_2Ni_{10}O_{18}$ |
| cryst color, habit | black opaque prism | dark brown long plate |
| cryst size (mm) | 0.42 × 0.22 × 0.20 | 0.40 × 0.15 × 0.05 |
| cryst system | monoclinic | triclinic |
| space group | $P2_1/c$ | $P\bar{1}$ |
| unit cell dimens | | |
| $a$ (Å) | 9.9390(2) | 9.795(1) |
| $b$ (Å) | 11.4488(2) | 11.295(1) |
| $c$ (Å) | 18.7425(3) | 11.413(2) |
| α (deg) | 90 | 117.96(1) |
| $\beta$ (deg) | 94.986(2) | 92.29(1) |
| $\gamma$ (deg) | 90 | 92.23(1) |
| $V$ (Å) | 2124.63(7) | 1112.0(2) |
| peaks to determine cell | 6484 | 40 |
| temp (K) | 133(2) | 148(2) |
| wavelength (Å) | 0.710 73 | 0.710 73 |
| $Z$ | 2 | 1 |
| fw | 1687.60 | 1715.65 |
| $D$ (calcd, g/cm$^3$) | 2.638 | 2.562 |
| abs coeff (mm$^{-1}$) | 12.639 | 12.076 |
| $F$(000) | 1604 | 818 |
| **Data Collection** | | |
| diffractometer | Siemens P4/CCD | Siemens P4 |
| $\theta$ range for data collcn (deg) | 2.06−25.98 | 2.02−22.50 |
| index ranges | $-12 \le h \le 11$ | $0 \le h \le 10$ |
| | $-6 \le k \le 13$ | $-10 \le k \le 10$ |
| | $-17 \le l \le 21$ | $-12 \le l \le 12$ |
| scan type | $\phi$ scan frames | Wyckoff $\omega$ |
| scan time or speed | 10 s/frame | variable (3−30 deg/min) |
| scan range | 0.3° in $\phi$ | 0.8° in $\omega$ |
| no. of reflcns collcd | 6981 | 3067 |
| no. of indepdt reflcns | 3630 ($R_{int}$ = 0.0235) | 2768 ($R_{int}$ = 0.0441) |
| **Solution and Refinement** | | |
| solution | direct methods | |
| refinement method | full-matrix least squares on $F^2$ | |
| H atoms | riding | |
| weighting scheme $a$, $b$[a] | 0.06720, 0 | 0.0720, 8.2746 |
| data/restraints/params | 3630/0/272 | 2766/34/281 |
| goodness-of-fit on $F^2$ | 1.268 | 1.060 |
| final $R^b$ indices [$I > 2\sigma(I)$] | $R_1(F)$ = 0.046 | $R_1(F)$ = 0.044 |
| | w$R_2(F^2)$ = 0.12 | w$R_2(F^2)$ = 0.11 |
| $R^b$ indices (all data) | $R_1(F)$ = 0.050, | $R_1(F)$ = 0.055, |
| | w$R_2(F^2)$ = 0.12 | w$R_2(F^2)$ = 0.12 |
| obsd data [$I > 2\sigma(I)$] | 3268 | 2379 |
| largest diff peak and hole (e Å$^{-3}$) | 3.80 and −6.17 | 2.46 and −2.26 |
| largest and mean Δ/esd | 0.001 and 0.000 | 0.000 and 0.000 |

[a] $w = 1/[\sigma^2(F_o^2) + (aP)^2 + bP]$; $P = [F_o^2 + 2F_c^2]/3$. [b] $R_1(F) = |\Sigma||F_o| - |F_c||/\Sigma|F_o|$; w$R_2(F^2) = [\Sigma[w_i(F_o^2 - F_c^2)^2]/\Sigma[w_i(F_o^2)^2]]^{1/2}$.

$[Ni_{10}(ER)_2(CO)_{18}]^{2-}$ members (E = P, As, Sb, Bi) also gives predicted values in agreement with the observed electron count.

Noteworthy is that the observed diamagnetism of **2** obtained from solid-state magnetic susceptibility measurements at room temperature is in harmony with the electron-counting models.

**Geometrical Analysis of the $[Ni_{10}(EMe)_2(CO)_{18}]^{2-}$ Dianions (E = Bi, Sb) Containing Empty Icosahedral $Ni_{10}E_2$ Cages with Corresponding Anions Containing Ni-Centered (Filled) $Ni_{10}E_2$ Icosahedral Cages. (a) $[Ni_{10}(BiMe)_2(CO)_{18}]^{2-}$ Dianion (2) versus the $[Ni_{11}Bi_2(CO)_{18}]^{3-}$ Trianion (4).** A geometrical comparison (Table 4) of the noncentered (empty) 1,12-$Ni_{10}Bi_2$ cage of pseudo $D_{5d}$ symmetry in the 150-electron $[Ni_{10}(BiMe)_2(CO)_{18}]^{2-}$ dianion (**2**) of the $[NMe_4]^+$ salt with the Ni-centered 1,12-$Ni_{10}Bi_2$ cage of pseudo $D_{5d}$ symmetry in the 159-electron $[Ni_{11}Bi_2(CO)_{18}]^{3-}$ trianion (**4**)[20] of the $[NEt_4]^+$ salt reveals major changes in the icosahedral $Ni_{10}Bi_2$ architecture resulting from the formal transformation of **2** into **4**; the interconversion involves the addition of the internal $d^{10}$ Ni(*i*) into the empty $Ni_{10}Bi_2$ cage (at the inversion center) with concomitant removal of the two one-electron Bi-attached methyl substituents and a negative ionic charge increase by one electron. This conceptual transformation of **2** into **4** causes a marked 1.1 Å elongation of the diameter of the highly compressed icosahedral cage of **2** along the principal 5-fold Bi···Bi′ axis from 3.9 Å in **2** to 5.0 Å in **4**. The resulting shape of the icosahedral cage thereby changes from an oblate spheroidal one in **2** to a nearly regular spherical one in **4**, as evidenced in **4** by the mean cage diameter of 5.2 Å along the five centrosymmetrically-related Ni(*s*)···Ni(*s*′) axes being nearly the same as that of 5.0 Å along the Bi···Bi′ axis. This considerable icosahedral-cage elongation along the pseudo-5-fold axis in **4** is caused by the formal insertion of the interior Ni(*i*) at the inversion center of the icosahedron, which gives rise to two identical short Ni(*i*)−Bi distances of 2.51 Å; the fact that this mean Ni(*i*)−Bi distance is 0.31 Å shorter than the mean Ni(*s*)−

(34) (a) King, R. B. *Inorg. Chim. Acta* **1992**, *198−200*, 841−861. (b) King, R. B. *Inorg. Chim. Acta* **1995**, *235*, 111−115. (c) King, R. B. *Polyhedron* **1994**, *13*, 2005−2016.

**Table 2. Comparative Geometrical Analysis of the Centrosymmetric $[Ni_{10}(EMe)_2(CO)_{18}]^{2-}$ Homologues (E = P,[a] As,[b] Sb,[c] Bi[d]) under Assumed $D_{5d}$ Symmetry with All Clusters as $[NMe_4]^+$ Salts**

| 1,12-$Ni_{10}E_2$ cage | $Ni_{10}P_2$ | $Ni_{10}As_2$ | $Ni_{10}Sb_2$ | $Ni_{10}Bi_2$ |
|---|---|---|---|---|
| A. Nonbonding Distances between Centrosymmetrically Related Cage Atoms (Å) | | | | |
| Ni(1)−Ni(1a) | 4.948(2) | 5.043(3) | 5.235(4) | 5.357(2) |
| Ni(2)−Ni(2a) | 4.866(2) | 4.974(3) | 5.142(3) | 5.275(2) |
| Ni(3)−Ni(3a) | 4.942(2) | 5.034(3) | 5.194(5) | 5.263(2) |
| Ni(4)−Ni(4a) | 4.956(2) | 5.037(3) | 5.184(3) | 5.248(2) |
| Ni(5)−Ni(5a) | 4.838(2) | 4.957(3) | 5.153(3) | 5.260(2) |
| Ni−Ni(av) | 4.91(av) | 5.01(av) | 5.18(av) | 5.28(av) |
| E(1)−E(1a) | 3.586(2) | 3.689(2) | 3.848(3) | 3.881(1) |
| B. Nickel−Pnicogen (E) Distances (Å) | | | | |
| E−Ni(1) | 2.375(2) | 2.450(2) | 2.576(2) | 2.638(1) |
| E−Ni(2) | 2.329(2) | 2.412(2) | 2.538(2) | 2.603(1) |
| E−Ni(3) | 2.366(2) | 2.431(2) | 2.575(2) | 2.635(1) |
| E−Ni(4) | 2.355(2) | 2.440(2) | 2.563(2) | 2.647(1) |
| E−Ni(5) | 2.324(2) | 2.405(2) | 2.538(2) | 2.610(1) |
| E−Ni(av) | 2.35(av) | 2.43(av) | 2.56(av) | 2.63(av) |
| C. Intrapentagonal Nickel−Nickel Distances (Å) | | | | |
| Ni(1)−Ni(2) | 2.636(1) | 2.731(2) | 2.873(2) | 2.985(2) |
| Ni(2)−Ni(3) | 2.575(1) | 2.635(2) | 2.709(2) | 2.757(2) |
| Ni(3)−Ni(4) | 2.622(1) | 2.712(2) | 2.856(2) | 2.932(1) |
| Ni(4)−Ni(5) | 2.584(1) | 2.621(2) | 2.731(2) | 2.731(1) |
| Ni(5)−Ni(1) | 2.660(1) | 2.731(2) | 2.863(2) | 2.977(2) |
| Ni−Ni(av) | 2.62(av) | 2.69(av) | 2.81(av) | 2.88(av) |
| D. Interpentagonal Nickel−Nickel Distances (Å) | | | | |
| Ni(1)−Ni(3a) | 2.505(2) | 2.502(2) | 2.519(2) | 2.516(2) |
| Ni(1)−Ni(4a) | 2.493(2) | 2.500(2) | 2.516(2) | 2.520(1) |
| Ni(2)−Ni(4a) | 2.538(2) | 2.510(2) | 2.524(2) | 2.515(2) |
| Ni(2)−Ni(5a) | 2.421(2) | 2.417(1) | 2.414(2) | 2.387(2) |
| Ni(3)−Ni(5a) | 2.497(2) | 2.522(2) | 2.507(2) | 2.539(2) |
| Ni−Ni(av) | 2.49(av) | 2.49(av) | 2.50(av) | 2.50(av) |
| E. Ni−CO Bridging Distances (Å) | | | | |
| Ni(1)−C(13) | 1.943(7) | 1.93(1) | 1.934(7) | 1.89(1) |
| Ni(1)−C(14) | 1.920(6) | 1.90(1) | 1.901(6) | 1.94(1) |
| Ni(3)−C(13a) | 1.897(7) | 1.86(1) | 1.883(6) | 1.88(1) |
| Ni(4)−C(14a) | 1.888(7) | 1.90(1) | 1.878(6) | 1.88(1) |
| Ni(2)−C(235a) | 2.123(7) | 2.26(1) | 2.221(6) | 2.32(1) |
| Ni(2)−C(245a) | 1.921(6) | 1.90(1) | 1.892(7) | 1.87(1) |
| Ni(3)−C(235a) | 1.991(6) | 1.95(1) | 2.008(7) | 1.95(1) |
| Ni(4)−C(245) | 1.967(6) | 1.96(1) | 1.966(7) | 1.98(1) |
| Ni(5)−C(235) | 1.944(6) | 1.91(1) | 1.887(6) | 1.88(1) |
| Ni(5)−C(245) | 2.262(6) | 2.19(1) | 2.339(6) | 2.15(1) |
| F. Ni−CO Terminal Distances (Å) | | | | |
| Ni(1)−C(1) | 1.775(7) | 1.81(1) | 1.783(6) | 1.80(1) |
| Ni(2)−C(2) | 1.769(6) | 1.76(1) | 1.749(6) | 1.78(1) |
| Ni(3)−C(3) | 1.796(7) | 1.78(1) | 1.789(7) | 1.82(1) |
| Ni(4)−C(4) | 1.792(7) | 1.77(1) | 1.766(7) | 1.80(1) |
| Ni(5)−C(5) | 1.753(8) | 1.76(1) | 1.758(6) | 1.77(1) |
| Ni−C(av) | 1.78(av) | 1.78(av) | 1.77(av) | 1.79(av) |
| G. C−O Bridging Distances (Å) | | | | |
| C(13)−O(13) | 1.16(1) | 1.17(1) | 1.14(1) | 1.19(1) |
| C(14)−O(14) | 1.17(1) | 1.15(1) | 1.16(1) | 1.16(1) |
| C(235)−O(235) | 1.17(1) | 1.17(1) | 1.16(1) | 1.19(1) |
| C(245)−O(245) | 1.17(1) | 1.20(1) | 1.17(1) | 1.19(1) |
| H. C−O Terminal Distances (Å) | | | | |
| C(1)−O(1) | 1.14(1) | 1.11(1) | 1.12(1) | 1.12(1) |
| C(2)−O(2) | 1.12(1) | 1.12(1) | 1.14(1) | 1.13(1) |
| C(3)−O(3) | 1.13(1) | 1.13(1) | 1.12(1) | 1.12(1) |
| C(4)−O(4) | 1.12(1) | 1.15(1) | 1.15(1) | 1.13(1) |
| C(5)−O(5) | 1.16(1) | 1.12(1) | 1.12(1) | 1.15(1) |
| | 1.13(av) | 1.13(av) | 1.13(av) | 1.13(av) |
| I. E−$CH_3$ Distance (Å) | | | | |
| E−C(Me) | 1.868(6) | 1.99(1) | 2.174(6) | 2.28(1) |
| J. Ni−E−Ni Angles (deg) | | | | |
| Ni(1)−E−Ni(2) | 68.5(1) | 68.3(1) | 68.36(4) | 69.42(4) |
| Ni(2)−E−Ni(3) | 66.1(1) | 65.9(1) | 63.98(5) | 63.50(3) |
| Ni(3)−E−Ni(4) | 67.8(1) | 67.7(1) | 67.56(5) | 67.44(3) |
| Ni(4)−E−Ni(5) | 66.4(1) | 65.5(1) | 64.73(4) | 62.59(3) |
| Ni(5)−E−Ni(1) | 68.6(1) | 68.5(1) | 68.09(6) | 69.12(3) |
| Ni−E−Ni(av) | 67.5(av) | 67.2(av) | 66.5(av) | 66.4(av) |
| K. Oblate Spheroidal Approximation of the $Ni_{10}E_2$ Core | | | | |
| minor: major semiaxes ratio | 0.657(11) | 0.671(7) | 0.687(6) | 0.682(10) |

[a] 22 °C/ref 41 (for the interatomic distances of the $Ni_{10}P_2$ cluster in the $[PPN]^+$ salt,[13] see ref 16). [b] 22 °C/ref 15. [c] −150 °C/ref 19. [d] −140 °C/this work.

**Table 3. Selected Interatomic Distances for the *closo*-1,12-Disubstituted Icosahedral $Ni_{10}Bi_2$ Cage in the Centrosymmetric $[NMe_4]_2[Ni_{10}(BiEt)_2(CO)_{18}]^{2-}$**

| dist between centrosymmetrically related core atoms | | intrapentagonal Ni−Ni dists | |
|---|---|---|---|
| Ni(1)−Ni(1a) | 5.307(3) | Ni(1)−Ni(2) | 3.019(2) |
| Ni(2)−Ni(2a) | 5.334(3) | Ni(2)−Ni(3) | 2.745(2) |
| Ni(3)−Ni(3a) | 5.232(3) | Ni(3)−Ni(4) | 2.874(2) |
| Ni(4)−Ni(4a) | 5.195(3) | Ni(4)−Ni(5) | 2.721(2) |
| Ni(5)−Ni(5a) | 5.272(3) | Ni(5)−Ni(1) | 2.973(2) |
| Ni−Ni(av) | 5.27(av) | Ni−Ni(av) | 2.87(av) |
| Bi(1)−Bi(1a) | 3.951(1) | | |
| Ni−Bi dists | | interpentagonal Ni−Ni dists | |
| Bi−Ni(1) | 2.609(2) | Ni(1)−Ni(3a) | 2.520(2) |
| Bi−Ni(2) | 2.652(2) | Ni(1)−Ni(4a) | 2.523(2) |
| Bi−Ni(3) | 2.621(2) | Ni(2)−Ni(4a) | 2.549(2) |
| Bi−Ni(4) | 2.625(2) | Ni(2)−Ni(5a) | 2.343(2) |
| Bi−Ni(5) | 2.640(2) | Ni(3)−Ni(5a) | 2.553(2) |
| Bi−Ni(av) | 2.63(av) | Ni−Ni(av) | 2.50(av) |

Bi distance of 2.82 Å in **4** implies the existence of strong radial Ni(*i*)−Bi bonding in **4**. One net consequence of the two Bi atoms strongly interacting with the interior Ni(*i*) in **4** is a substantial weakening in their surface−cage bonding interactions with the 10 surface Ni(*s*) atoms, as indicated by a 0.19 Å increase of the mean Ni(*s*)−Bi distance from 2.63 Å in **2** to 2.82 Å in **4**.

Other salient structural consequences due to the formal insertion of the Ni(*i*) into the empty icosahedral $Ni_{10}Bi_2$ cage of **2** at the inversion center are a small decrease of 0.05 Å in the mean inversion center (IC)-to-Ni(*s*) distance and a corresponding small decrease of 0.07 Å in the mean intrapentagonal Ni(*s*)−Ni(*s*′) distance. These geometrical changes are consistent with the view that the bonding interactions between the Ni(*i*) and the 10 Ni(*s*) atoms in **4** are relatively weak compared to the strong bonding Ni(*i*)−Bi interactions. If the radial Ni(*i*)−Ni(*s*) bonding in **4** were also strong, one would expect weaker surface−cage Ni(*s*)−Ni(*s*′) bonding interactions and hence longer (instead of the observed shorter) Ni(*s*)−Ni(*s*′) distances in **4** versus those in **2**. The corresponding change in the mean interpentagonal Ni(*s*)−Ni(*s*′) is only 0.01 Å; this invariance of the mean value for the 10 interpentagonal Ni(*s*)−Ni(*s*′) distances, whether the icosahedral cage is empty or filled, may be attributed to the dispositions of the 8 bridging carbonyl ligands in both **2** and **4**.

In the $C_i$-$\bar{1}$ $[Ni_{11}Bi_2(CO)_{18}]^{3-}$ trianion[20] the 8 bridging COs of the 18 carbonyl ligands adopt a different centrosymmetric mode of coordination to the 10 Ni(*s*) atoms from that found for all of the other $[Ni_{10}(ER)_2(CO)_{18}]^{2-}$ dianions (E = P, As, Sb, Bi) under the same pseudo $C_{2h}$-2/*m* symmetry. Again, there are 10 terminal COs, one per surface Ni(*s*), and 8 bridging COs in the equatorial region of the cluster. However, the bridging COs now consist of 6 edge-bridging COs and 2 face-capping COs. The 2 triply bridging COs cap the opposite (centrosymmetrically related) triangular $Ni_3$ faces, each of which consists of 1 *intrapentagonal* and 2 *interpentagonal* edges; the remaining 6 doubly bridging COs span the other 6 *interpentagonal* edges (*i.e.*, those not belonging to the two OC-capped trinickel faces). The pseudo horizontal mirror plane passes through the 2 triply bridging COs, the Ni(*i*), the 2 Bi, and 2 Ni(*s*) atoms,

**Table 4. Analysis of Selected Mean Distances (Å) of the Homologous $[Ni_{10}(EMe)_2(CO)_{18}]^{2-}$ Dianions (E = Bi (2), Sb) Containing Empty Icosahedral 1,12-$Ni_{10}E_2$ Cages with the $[Ni_{11}Bi_2(CO)_{18}]^{3-}$ Trianion (4) and the $[Ni_{11}(SbNi(CO)_{18})]^{n-}$ Dianion ($n$ = 2) and Trianion ($n$ = 3), Containing Ni-Centered (Filled) Icosahedral 1,12-$Ni_{10}E_2$ Cages**

| | $Ni_{10}Bi_2$ dianion[a] | $Ni_{11}Bi_2$ trianion[b] | $Ni_{10}Sb_2$ dianion[c] | $Ni_{11}Sb_2$ dianion[d] | $Ni_{11}Sb_2$ trianion[e] |
|---|---|---|---|---|---|
| empty/filled 1,12-$Ni_{10}E_2$ cage | empty $Ni_{10}Bi_2$ | filled $Ni_{10}Bi_2$ | empty $Ni_{10}Sb_2$ | filled $Ni_{10}Sb_2$ | filled $Ni_{10}Sb_2$ |
| IC−E[f] [2][g] | 1.95 | 2.51 | 1.92 | 2.40 | 2.40 |
| IC−Ni(*s*)[f] [10] | 2.64 | 2.59 | 2.60 | 2.57 | 2.58 |
| Ni(*s*)−E [10] | 2.63 | 2.82 | 2.56 | 2.73 | 2.74 |
| intrapentagonal Ni(*s*)−Ni(*s*′) [10] | 2.88 | 2.81 | 2.81 | 2.77 | 2.78 |
| interpentagonal Ni(*s*)−Ni(*s*′) [10] | 2.50 | 2.51 | 2.50 | 2.52 | 2.52 |

[a] $[NMe_4]^+$/this work. [b] $[NEt_4]^+$/ref 20. [c] $[NMe_4]^+$/ref 19. [d] $[N(PPh_3)_2]^+$/ref 18. [e] $[NMe_3(CH_2Ph)]^+$/ref 18. [f] IC denotes the inversion center of the icosahedral $Ni_{10}E_2$ cage, which for a Ni-centered (filled) icosahedron is occupied by the interior Ni(*i*). [g] Values in brackets denote the number of equivalent distances under assumed $D_{5d}$ symmetry having each mean value in the right row.

while the pseudo-2-fold axis passes through 2 doubly bridging COs and the Ni(*i*). The pseudo-$C_2h$-2/*m* symmetry exhibited by the 18-vertex carbonyl polyhedron gives rise to three independent Ni(*s*) atoms, corresponding to 3 independent Ni(*s*)−Bi edges and 3 independent intrapentagonal and 3 interpentagonal Ni(*s*)−Ni(*s*′) edges. The other 8 intrapentagonal Ni(*s*)−Ni(*s*′) edges are not connected by either edge- or face-bridging COs. The marked influence of the bridging COs on the bond-length shortening of certain Ni(*s*)−Ni(*s*′) edges is readily apparent; the only independent *intrapentagonal* Ni(*s*)−Ni(*s*′) edge involved with a bridging CO (*viz.*, the face-capping CO) is 0.11 Å shorter than the mean of 2.81 Å for the 5 independent *intrapentagonal* Ni(*s*)−Ni(*s*′) edges; the 5 independent *interpentagonal* Ni(*s*)−Ni(*s*′) edges, each of which is carbonyl-linked, are all within 0.02 Å of the 0.3 Å-shorter mean of 2.51 Å. Albano, *et al.*[20] pointed out that this different carbonyl arrangement in the $[Ni_{11}Bi_2(CO)_{18}]^{3-}$ trianion gives rise to 3 COs (one terminal and two bridging) being coordinated to 8 Ni(*s*) atoms but only 2 COs (one terminal and one triply bridging) being linked to the other 2 centrosymmetrically related Ni(*s*) atoms on the pseudo mirror plane; from the observation that a face-capping CO is 0.3 Å nearer to each of these mirror-containing Ni(*s*) atoms and thereby forms a stronger Ni−($\mu_3$-CO) bonding interaction, they concluded that each of the 10 surface Ni(*s*) atoms has an approximately equivalent charge density.

**(b) $[Ni_{10}(SbMe)_2(CO)_{18}]^{2-}$ Dianion versus the $[Ni_{11}\{SbNi(CO)_3\}_2(CO)_{18}]^{n-}$ Dianion ($n$ = 2) and Trianion ($n$ = 3).** Table 4 also allows a geometrical comparison of selected mean distances (under pseudo-$D_{5d}$ symmetry) between the noncentered (empty) icosahedral 1,12-$Ni_{10}Sb_2$ cage in the 150-electron $[Ni_{10}(SbMe)_2(CO)_{18}]^{2-}$ homologue[19] of **2** and the corresponding Ni-centered (filled) icosahedral 1,12-$Ni_{10}Sb_2$ cage in the crystallographically determined 158-electron dianion ($n$ = 2) and 159-electron trianion ($n$ = 3) of the $[Ni_{11}(SbNi(CO)_3)_2(CO)_{18}]^{n-}$ series ($n$ = 2−4).[18] In each of these anions the Sb-attached $Ni(CO)_3$ substituent is coordinated as a Lewis-acid adduct to the otherwise lone electron pair of each Sb (corresponding to the formation of a dative electron-pair bond). Hence, the same charged anions in the $[Ni_{11}Bi_2(CO)_{18}]^{n-}$ series ($n$ = 2−4)[20] and $[Ni_{11}(SbNi(CO)_3)_2(CO)_{18}]^{n-}$ series ($n$ = 2−4)[18] have the same observed number of metal cluster valence electrons (CVEs). Especially noteworthy is that the 18 carbonyl ligands in both the $[Ni_{11}\{SbNi(CO)_3\}_2(CO)_{18}]^{n-}$ dianion ($n$ = 2) and trianion ($n$ = 3) possess the same pseudo-$C_{2h}$ distribution of bridging COs (*viz.*, 4 doubly and 4 triply bridging) as found in the $[Ni_{10}(SbMe)_2(CO)_{18}]^{2-}$ dianion and its homologues including **2**.

First, it should be noted from Table 4 that the corresponding mean distances are experimentally equivalent (within 0.01 Å) for the 158-electron dianion ($n$ = 2) and 159-electron trianion ($n$ = 3) of the $[Ni_{11}(SbNi(CO)_3)_2(CO)_{18}]^{n-}$ series ($n$ = 2−4). This indicated invariance of geometry to the negative ionic charge of the anions in this series suggests that the structurally determined Ni-centered $Ni_{10}Bi_2$ cage geometry for the 159-electron trianion ($n$ = 3) in the corresponding $[Ni_{11}Bi_2(CO)_{18}]^{n-}$ series ($n$ = 2−4) is essentially unchanged for the other two members. Second, the conceptual interconversion of the empty icosahedral $Ni_{10}Sb_2$ cage in the $[Ni_{10}(SbMe)_2(CO)_{18}]^{2-}$ dianion into the Ni-filled one in the $[Ni_{11}(SbNi(CO)_3)_2(CO)_{18}]^{2-}$ dianion similarly produces a large 0.96 Å elongation of the diameter of the highly compressed icosahedral cage along the principal 5-fold Sb···Sb′ axis. However, the resulting Ni-filled cage diameter of 4.80 Å along the Sb···Sb′ axis is still 0.34 Å smaller than the mean cage diameter of 5.14 Å along the five centrosymmetrically related Ni(*s*)···Ni(*s*′) axes. In this case, the Ni-filled icosahedral cage in the $Ni_{11}Sb_2$ dianion is still somewhat oblate.

Otherwise, Table 4 shows that the observed trends resulting from the formal transformation of the $Ni_{10}Sb_2$ dianion into the $Ni_{11}Sb_2$ dianion (which includes the placement of the internal Ni(*i*) at the inversion center of the icosahedral cage) parallel those resulting from the similar conversion of the $Ni_{10}Bi_2$ dianion (**2**) into the $Ni_{11}Bi_2$ dianion (**4**). These analogous trends are as follows: (1) two short radial Ni(*i*)−Sb distances of 2.40 Å indicative of strong radial Ni(*i*)−Sb bonding; (2) the 10 Ni(*s*)−Sb distances being 0.17 Å—longer than those in the empty icosahedral cage, corresponding to much weaker surface−cage Ni(*s*)−Sb bonding due to the additional involvement of the Sb atoms in strong radial bonding with the interior Ni(*i*); (3) small decreases of 0.02 Å in the IC-to-Ni(*s*) distances and 0.04 Å in the intrapentagonal Ni(*s*)−Ni(*s*′) distances, indicating that the interior Ni(*i*) forms relatively weak bonding interactions with the 10 surface Ni(*s*) atoms and therefore has little effect on surface−cage *intrapentagonal* Ni(*s*)−Ni(*s*′) bonding; (4) the analogous mean *interpentagonal* Ni(*s*)−Ni(*s*′) distances of 2.50 Å in the $Ni_{10}Sb_2$ dianion and 2.52 Å in the $Ni_{11}Sb_2$ dianions comparing favorably (within 0.02 Å) with those in the corresponding $Ni_{10}Bi_2$ and $Ni_{11}Bi_2$ dianions. In fact, the mean *interpentagonal* Ni(*s*)−Ni(*s*′) distances in these and the two other homologous $[Ni_{10}(EMe)_2(CO)_{18}]^{2-}$ dianions (E = P, As)

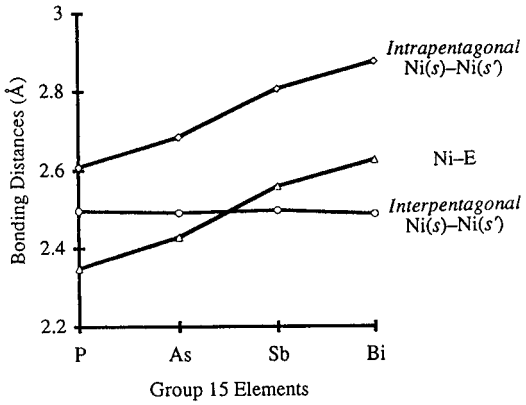


**Figure 3.** Plot showing the variation of the mean distances for each of the three kinds of five independent icosahedral edges in the centrosymmetric 1,12-$Ni_{10}E_2$ icosahedral cage as a function of the congeneric E element for the four members of the homologous $[Ni_{10}(EMe)_2(CO)_{18}]^{2-}$ series (E = P, As, Sb, Bi). The means of the Ni−E edges (Δ) and *intrapentagonal* Ni(*s*)−Ni(*s*′) edges (◇) increase in a similar fashion with the increased sizes of the main-group V (15) E atoms (*i.e.*, nonpolar covalent radii[35] are 1.10 Å for P, 1.19 Å for As, 1.38 Å for Sb, and 1.46 Å for Bi). In sharp contrast, the means of the *interpentagonal* Ni(*s*)−Ni(*s*′) edges (○) are essentially invariant to the increased sizes of the four different pairs of E atoms that cap the two pentagonal Ni(*s*) faces; the uniformity of these considerably shorter means is attributed to the analogous arrangements in the four members of the 8 bridging COs that span all of the *interpentagonal* Ni(*s*)−Ni(*s*′) edges.

are alike (within 0.03 Å) as well as much shorter than the *intrapentagonal* Ni(*s*)−Ni(*s*′) distances (which, in contrast, uniformly increase from 2.62 Å for E = P to 2.88 Å for E = Bi); these structural observations are readily ascribed to the analogous polyhedral arrangements of the 18 COs and in particular to the bond-length shortening effects of the 8 bridging carbonyls. The considerable variations that occur in individual distances are due primarily to the carbonyl ligands in a given cluster conforming, in general, to only pseudo-$C_{2h}$ symmetry instead of the pseudo $D_{5d}$ symmetry assumed in Table 4 for each icosahedral 1,12-$Ni_{10}E_2$ cage (E = Bi, Sb). Nevertheless, the observed systematic trends in mean values based upon averaging equivalent distances under $D_{5d}$ symmetry provide a self-consistent representation of the structural/bonding features of this important class of $Ni_xE_y$ icosahedral clusters.

**Comparison of the Four Homologous $[Ni_{10}(EMe)_2(CO)_{18}]^{2-}$ Members (E = P, As, Sb, Bi) and Resulting Implications. (a) Geometrical Features.** Because each member of the $[Ni_{10}(ER)_2(CO)_{18}]^{2-}$ series (E = P,[13] As,[15] Sb,[19] Bi) in all structurally determined salts invariably possesses a crystallographic inversion center, only one-half of the 30 icosahedral edges in each $Ni_{10}E_2$ cage are independent. Table 4 presents a comparison of selected distances under assumed $D_{5d}$ symmetry for the $[NMe_4]^+$ salts of the four centrosymmetric $[Ni_{10}(EMe)_2(CO)_{18}]^{2-}$ members (E = P, As, Sb, Bi) which differ from one another only by the group V (15) E element. Figure 3 gives a plot showing the variation of the mean distances for each of the five independent Ni(*s*)−E, *intrapentagonal* Ni(*s*)−Ni(*s*′), and *interpentagonal* Ni(*s*)−Ni(*s*′) edges in a given 1,12-$Ni_{10}E_2$ cage as a function of the congeneric E element.

The geometries of these dianions are very similar; each dianion conforms closely to pseudo $C_{2h}$-2/*m* symmetry. The pseudo horizontal mirror plane passes through the 2 E and 2 Ni(*s*) atoms; no atoms lie on the perpendicular twofold principal axis. Both Table 4 and Figure 3 show the following trends under assumed $D_{5d}$ symmetry: (1) the empty 1,12-$Ni_{10}E_2$ icosahedral cage is similarly deformed for all four members by a large oblate compression along the pseudo-5-fold E···E′ axis. The nonbonding E···E′ distances among the empty $Ni_{10}P_2$ (3.59 Å), $Ni_{10}As_2$ (3.69 Å), $Ni_{10}Sb_2$ (3.85 Å), and $Ni_{10}Bi_2$ (3.88 Å) cages are much less than the five centrosymmetrically related, nonbonding mean Ni(*s*)−Ni(*s*′) distances of 4.91, 5.01, 5.18, and 5.28 Å, respectively. (2) The means of the five independent Ni(*s*)−E edges and five independent *intrapentagonal* Ni(*s*)−Ni(*s*′) edges in the four $Ni_{10}E_2$ icosahedral cages increase in an analogous fashion with the increased size of the main-group V (15) E atoms. Subtraction of the nonpolar covalent radii[35] for P (1.10 Å), As (1.19 Å), Sb (1.38 Å), and Bi (1.46 Å) from the corresponding mean Ni(*s*)−E distances gives decreasing values of 1.25, 1.24, 1.18, and 1.17 Å, respectively, for the covalent nickel radius. (3) The means of the five independent *interpentagonal* Ni(*s*)−Ni(*s*′) edges are invariant to the increased sizes of the different E atoms capping each pentagonal face; the observed means of 2.49−2.50 Å are in agreement with that found[36] in ccp nickel metal (2.492 Å).

The 18 carbonyl ligands in each dianion are distributed in an identical fashion about the 1,12-$Ni_{10}E_2$ cage. The 10 terminal COs are each coordinated to one surface Ni(*s*) atom. The 8 bridging COs, consisting of 4 doubly and 4 triply bridging COs, are arranged under pseudo-$C_{2h}$ symmetry in alternating pairs of two doubly (*d*) and two triply (*t*) bridging COs (*i.e.*, corresponding to a cyclic *dttddttd* CO sequence) on adjacent interpentagonal edges and triangular faces formed by one intrapentagonal and two interpentagonal edges. This particular distribution of 18 terminal and bridging COs gives rise to 30 carbonyl links (*i.e.*, one for each terminal CO, two for each edge-bridging CO, and three for each face-capping CO), such that each of the 10 surface Ni(*s*) atoms is similarly connected to 3 COs (one terminal and two bridging). This centrosymmetric carbonyl arrangement results in each of the 10 *interpentagonal* Ni(*s*)−Ni(*s*′) edges being linked by a doubly bridging CO or by one or two triply bridging COs; 4 of the 10 *intrapentagonal* Ni(*s*)−Ni(*s*′) edges are linked by one triply bridging CO. Table 4 reveals similar effects of the bridging COs in markedly shortening certain individual *intrapentagonal* and *interpentagonal* Ni(*s*)−Ni(*s*′) edges in the four homologues from the mean values under assumed $D_{5d}$ symmetry for the $Ni_{10}E_2$ cage.

The shape of the icosahedral framework of the 12 $Ni_{10}E_2$ cage atoms was found for each member of the $[Ni_{10}(EMe)_2(CO)_{18}]^{2-}$ series (E = P, As, Sb, Bi) from use of the crystallographic Ni−E and centrosymmetric E···E′ and Ni···Ni′ distances to approximate an oblate spheroid with the smaller minor axis (2*c*) coinciding with the E···E′ axis and the other two larger orthogonal major axes (2*a* = 2*b*) lying in the equatorial plane of the $Ni_{10}E_2$ cage. The shape of the oblate spheroid is defined in terms of the minor (*c*)-to-major (*a*) semiaxial ratio, where the length *c* of the minor semiaxis corresponds to one-half the E···E′ distance; the length *a* for

(35) Purcell, K. F.; Kotz, J. C. *Inorganic Chemistry*; W. B. Saunders: Philadelphia, 1977.
(36) Donohue, J. *The Structures of the Elements*; John Wiley and Sons: New York, 1974; p 213.

the two equivalent major semiaxes was calculated from the crystallographic distances.[37] The differences in oblate compression along the four icosahedral $Ni_{10}E_2$ frameworks determined from the calculated mean *c*/*a* shape ratios are surprisingly small; although slight increases are observed on going from E = P (0.657) to E = As (0.671) and then to E = Sb (0.687), a slight decrease then occurs for E = Bi (0.682).

If the primary cause of a cage deformation involved only size effects, then the $Ni_{10}E_2$ cages would be expected to become more prolate spheroids as E becomes larger. Thus, combined electronic−size effects need to be considered in order to account for the observation of the relatively invariant oblate compressions for the four cages. The aforementioned lengthening of the Ni−E bonds with larger E atoms, which is due primarily to the increase of the E covalent radii, is also paralleled by a similar increase of the *intrapentagonal* Ni−Ni bond lengths, leading to relatively constant Ni−E−Ni angles of *ca*. 67° for the four $Ni_{10}E_2$ icosahedra. In a $M_2E_2$-bridged system the M−E−M angles are governed not only by the minimization of all nonbonded repulsions between atoms which depend on their sizes but also by interorbital electron-pair interactions, which for a more electronegative bridging atom favor a wider bridging angle.[38] Thus, the observed sizes and shapes of the oblate spheroidal $Ni_{10}E_2$ frameworks are dictated by combined electronic/steric effects including the steric effects of the ligand polyhedra. This analysis emphasizes that the Ni−E connectivities are much stronger than the intrapentagonal Ni−Ni connectivities in the $Ni_{10}E_2$ cages. This is evidenced by concomitant lengthening of the *intrapentagonal* Ni−Ni distances upon the increase in Ni−E distances with a larger E atom in order to maintain relatively constant Ni−E−Ni angles. If these Ni−Ni distances did not increase, then the $Ni_{10}Sb_2$ and $Ni_{10}Bi_2$ cages would have considerably more prolatelike ellipsoidal shapes along with implausibly acute Ni−E−Ni angles of 55.0 and 53.6°, respectively.

**(b) Stereochemical Isomers.** A prime trend is that for E = P and As three different types of electronically equivalent (isolobal) $[Ni_{12-x}(ER)_x(CO)_{24-3x}]^{2-}$ members ($x$ = 2−4) containing noncentered 1,12-$Ni_{10}E_2$, 1,2,12-$Ni_9E_3$, and 1,2,9,12-$Ni_8E_4$ icosahedral cages were isolated and structurally characterized; in contrast, for E = Sb and Bi only the $[Ni_{10}(ER)_2(CO)_{18}]^{2-}$ members are known despite extensive unsuccessful attempts to detect the other two types. For example, reactions of $[Ni_6(CO)_{12}]^{2-}$ (**1**) with $MePCl_2$ have produced the $[Ni_{10}(PMe)_2(CO)_{18}]^{2-}$, $[Ni_9(PMe)_3(CO)_{15}]^{2-}$, and $[Ni_8(PMe)_4(CO)_{12}]^{2-}$ dianions;[13] similarly, reactions of **1** with $RAsCl_2$ reagents have given rise to the $[Ni_{10}(AsMe)_2(CO)_{18}]^{2-}$ and $[Ni_9(AsPh)_3(CO)_{15}]^{2-}$ dianions[15] and the $[Ni_8(As^tBu)_4(CO)_{12}]^{2-}$ dianion.[28] It is likely that the presumed nonexistence of the corresponding antimony or bismuth clusters with either empty 1,2,12-$Ni_9E_3$ or 1,2,9,12-$Ni_8E_4$ cages is a consequence of the empty icosahedral cage being thermodynamically unstable due largely to the resulting effects of the longer and weaker Sb−Sb and Bi−Bi bonds on the icosahedral cage architectures.

In opposition to the two main-group V (15) atoms in the empty or Ni-centered $Ni_{10}E_2$ icosahedral cages being invariably located at opposite 1,12-vertices, the two E atoms in disubstituted isolobal main-group V (15) derivatives of the regular icosahedral $[B_{12}H_{12}]^{2-}$ dianion occupy adjacent 1,2-vertices. Specifically, Todd, Little, and their co-workers[39] have systematically prepared and characterized 1,2-$E_2B_{10}H_{10}$ derivatives (E = P, As, Sb, Bi) as well as mixed 1,2-$EBiB_{10}H_{10}$ derivatives (E = P, As, Sb). An X-ray diffraction analysis of $Bi_2B_{10}H_{10}$ revealed a highly distorted $C_{2v}$ icosahedral cage with 1 Bi−Bi edge of 2.96 Å, 8 Bi−B edges of 2.48 Å (av), and 21 B−B edges of 1.80 Å (av).[39d]

Of the three possible disubstituted $A_{10}E_2$ icosahedral isomers (*viz*., the $C_{2v}$ 1,2-, the $C_{2v}$ 1,7-, and the $D_{5d}$ 1,-12-), it is apparent from stereochemical considerations that the symmetrical $D_{5d}$ 1,12-isomer would best minimize cage-strain and thereby would be thermodynamically the most stable isomer. Furthermore, only the $D_{5d}$ 1,12-isomer for both empty or Ni-centered $Ni_{10}E_2$ icosahedral cages would give rise to suitable polyhedral ligand arrangements (*i.e*., the observed ones) for the 10 terminal and 8 bridging COs to coordinate in a favorable steric/electronic fashion to the 10 surface Ni(*s*) atoms with a resulting equivalent localized charge density on each Ni(*s*). In the case of the $E_2B_{10}H_{10}$ derivatives,[39] the synthetic methodology allows formation of only the known 1,2-isomers. In light of its highly deformed icosahedral framework, the observed behavior of the 1,2-$Bi_2B_{10}H_{10}$, in being thermally stable in the solid state up to 350 °C (before darkening) and in giving rise to an ion-parent peak in an EI mass spectrum, is especially surprising.[39d] One can conclude that its existence is due to the B−B and B−Bi bonding interactions being sufficiently strong and its 10 hydrogen atoms not sterically demanding to offset the presumed large icosahedral cage-strain created by the much longer Bi−Bi bonding edge.

**Experimental Analyses of the $[Ni_{10}(EMe)_2(CO)_{18}]^{2-}$ Dianions (E = P, As, Sb, Bi) and Resulting Implications. (a) Infrared Spectra Analyses.** The virtually identical IR spectra of both the 150-electron **2** and **3** in THF exhibited a strong terminal carbonyl absorption at 2010 (2005) $cm^{-1}$ and a broad medium carbonyl absorption at 1829 (1830) $cm^{-1}$ that can be ascribed to edge-bridging COs; in contrast to the three-band carbonyl pattern observed for the phosphorus homologue (but not for the arsenic and antimony homologues), no distinct maximum characteristic of face-bridging COs was observed in either **2** or **3**.

A comparison of the infrared solution spectra of the $[Ni_{10}(EMe)_2(CO)_{18}]^{2-}$ dianions (E = P, As, Sb, Bi) reveals

(37) The length *a* of the two major semiaxes (for which $a = b$) of the spheroid was calculated from the equation $a = [(c^2 \sin^2\theta)/((c/r) - \cos^2\theta)]^{1/2}$, where *c* is the length of the minor semiaxis corresponding to one-half of the E···E′ distance, *r* is a vector from the centroid of the spheroid to each Ni atom corresponding to one-half of the centrosymmetric Ni···Ni′ distance, and $\theta$ is the dihedral angle between the centroid-to-E vector and the centroid-to-Ni vector. The dihedral $\theta$ angle was calculated from trigonometric relationship $h^2 = r^2 + c^2 - 2cr\cos\theta$, where *h* denotes the Ni−E bonding distance. The small deviations (±0.04 Å) obtained for the five individual crystallographically independent Ni atoms in each of the four $Ni_{10}E_2$ clusters provides the basis for our premise that the ellipsoidal shape ($a \neq b \neq c$) for each icosahedral $Ni_{10}E_2$ framework is closely approximated to an oblate spheroid ($a = b > c$). The mean *c*/*a* shape ratios are 1.793 Å/2.728 Å = 0.657 for E = P, 1.845 Å/2.749 Å = 0.671 for E = As, 1.924 Å/2.801 Å = 0.687 for E = Sb, and 1.941 Å/2.845 Å = 0.682 for E = Bi.

(38) Dahl, L. F.; Rodulfo de Gil, E.; Feltham, R. D. *J. Am. Chem. Soc*. **1969**, *91*, 1653−1664.

(39) (a) 1,2-$P_2B_{10}H_{10}$: Little, J. L.; Kester, J. G.; Huffman, J. C.; Todd, L. J. *Inorg. Chem*. **1989**, *28*, 1087−1091. (b) 1,2-$As_2B_{10}H_{10}$: Hanusa, T. P.; Roig de Parisi, N.; Kester, J. G.; Arafat, A.; Todd, L. J. *Inorg. Chem*. **1987**, *26*, 4100−4102. (c) 1,2-$Sb_2B_{10}H_{10}$: Little, J. L. *Inorg. Chem*. **1979**, *18*, 1598−1600. (d) 1,2-$Bi_2B_{10}H_{10}$ and 1,2-$EBiB_{10}H_{10}$: Little, J. L.; Whitesell, M. A.; Kester, J. G.; Folting, K.; Todd, L. J. *Inorg. Chem*. **1990**, *29*, 804−808.

insignificant variations of the two higher-frequency absorption maxima in the carbonyl region. In THF solution, these four homologues with E = P, As, Sb, and Bi exhibited one strong terminal carbonyl absorption at 2012, 2005, 2007, and 2010 $cm^{-1}$, respectively, and one broad medium edge-bridging carbonyl absorption at 1830, 1840, 1829, and 1829 $cm^{-1}$, respectively. It is apparent that the nature of the group V (15) E atoms does not significantly alter the average negative charge density on the surface Ni(*s*) atoms of the empty icosahedral 1,12-$Ni_{10}E_2$ cage; a significant increase in the relative negative charge density on the Ni(*s*) atoms would be expected to increase $d_\pi$(Ni(*s*))$-\pi^*$(CO) backbonding and thereby lower the terminal carbonyl frequency of the cluster.

A comparison of the IR spectra of **2** and **3** with the reported IR spectra of the $[Ni_{11}Bi_2(CO)_{18}]^{n-}$ anions ($n$ = 2−4) is also of interest in assessing the combined electronic effects of the aforementioned structural differences and the varying anionic charge of the Ni-centered anions. For the $[Ni_{11}Bi_2(CO)_{18}]^{n-}$ anions ($n$ = 2−4), Longoni and co-workers[20] reported that the 158-electron dianion ($n$ = 2) in acetonitrile displayed infrared carbonyl absorptions at 1995 (s), 1840 (m), and 1780 (sh, br) $cm^{-1}$ which were attributed to terminal edge-bridging, and face-bridging COs, respectively; the 159-electron trianion ($n$ = 3) in acetonitrile expectedly showed much lower frequencies at 1963 (s), 1807 (s), and 1740 (sh, br) $cm^{-1}$. The terminal carbonyl frequency for the 150-electron noncentered $Ni_{10}Bi_2$ carbonyl dianion (**2**) is 15 $cm^{-1}$ higher than that for the 158-electron Ni-centered $Ni_{10}Bi_2$ carbonyl dianion ($n$ = 2), but the bridging frequency is 12 $cm^{-1}$ lower. Because the overall negative ionic charge (−2) is the same, we conclude that the net electronic effect resulting from the formal transformation of **2** into the $[Ni_{11}Bi_2(CO)_{18}]^{2-}$ dianion (*via* the formal insertion of the $d^{10}$ Ni(*i*) into the icosahedral $Ni_{10}Bi_2$ cavity and the concomitant removal of the two Bi-attached alkyl substituents) does not markedly change the average localized negative charge density on the Ni(*s*) atoms.

**(b) Electrochemical Analyses.** Cyclic voltammograms of three homologous $[Ni_{10}(EMe)_2(CO)_{18}]^{2-}$ members (E = P, Sb, Bi) in THF (for E = P) or acetonitrile (for E = Sb, Bi) did not exhibit any reversible reduction out to −1.5 V. However, these CVs each displayed an irreversible oxidation wave at *ca.* +0.75 V for E = P,[13] +0.60 V for E = Sb,[19] and +0.70 V for E = Bi, which indicates that each cluster undergoes a significant architectural rearrangement or decomposition upon oxidation. The observed insignificant variations in the irreversible oxidation waves are also consistent with the IR data in indicating that no marked changes in the surface charge density occur on the icosahedral 1,12-$Ni_{10}E_2$ cage upon formal substitution of the group V (15) E atoms.

**(c) NMR Spectral Analysis.** A $^1H$ NMR spectrum of $[NMe_4]_2$[**2**] in acetone-$d_6$ at room temperature showed signals corresponding to the methyl groups attached to the bismuth atoms and those of the $[NMe_4]^+$ counterions; the signals integrated closely to the theoretical 6:24 ratio. The $[NMe_4]^+$ proton resonance at $\delta$ 3.46 ppm is near that at $\delta$ 3.21 ppm for $[NMe_4]$Br. The methyl substituent signal at 2.37 ppm compares favorably with that of $\delta$ 2.40 ppm for E = P and that of 1.10 ppm for E = Sb in the $[Ni_{10}(EMe)_2(CO)_{18}]^{2-}$ homologues (also as $[NMe_4]^+$ salts); it is likewise close to that at $\delta$ 2.53 ppm for the methyl substituent in the 36-electron $Fe_2(CO)_8(\mu_2\text{-}BiMe)_2$.[40]

A room-temperature $^{13}C\{^1H\}$ NMR spectrum of $[NMe_4]_2$[**2**] in acetone-$d_6$ displayed two resonances assigned to the $[NMe_4]^+$ counterions and the Bi-attached methyl substituents. Signals due to the carbonyl ligands were not detected at room temperature on account of fast terminal−bridge carbonyl exchange. However, a limiting slow-exchange $^{13}C\{^1H\}$ NMR spectrum was obtained at −60 °C; two sharp resonances at 193.8 ppm (assigned to the terminal carbonyls) and 249.4 ppm (assigned to the unresolved doubly and triply bridging carbonyls) were observed along with the two resonances at −8.7 and 54.3 ppm due to the Bi-attached methyl substituents and methyl groups of the $[NMe_4]^+$ counterions, respectively.

Similar limiting slow-exchange $^{13}C\{^1H\}$ NMR spectra (with respect to terminal−bridge carbonyl exchange) were previously observed for two $[Ni_{10}(EMe)_2(CO)_{18}]^{2-}$ homologues (E = P,[41] Sb[19]) as $[NMe_4]^+$ salts. The spectrum at −80 °C for E = P consisted of two sharp resonances at 190.2 ppm (terminal COs) and 241.4 ppm (bridging COs) along with a resonance at 25.8 ppm (P-attached methyl substituents);[41] a corresponding spectrum at −60 °C for E = Sb also gave two sharp resonances at 191.8 ppm (terminal COs) and 240.8 ppm (bridging COs) together with a resonance at −4.2 ppm (Sb-attached $CH_3$ substituents).[19]

These limiting slow-exchange $^{13}C\{^1H\}$ spectra are completely consistent with those obtained at −80 °C and interpreted by Longoni, Heaton, and Chini[42] for $[Ni_5(CO)_{12}]^{2-}$, $[Ni_6(CO)_{12}]^{2-}$, $[Ni_9(CO)_{18}]^{2-}$, and $[Ni_{12}(CO)_{21}H_{4-n}]^{n-}$ ($n$ = 2,3); resonances for the terminal COs ranged from 192 to 203 ppm, while those for the doubly bridging COs ranged from 230 to 257 ppm.

**(d) Mass Spectral Analysis.** A negative-ion mass spectrum of $[NMe_4]_2$[**2**] was obtained via the electrospray ionization (ESI) method.[43] Signals corresponding to 8 relatively abundant doubly charged ion-fragments were observed. The assignment of each ion-fragment formula was based upon the resulting simulated isotopic pattern matching the observed one for each signal.[44] No signal corresponding to the doubly charged ion-parent, $[M]^{2-}$, was detected. Nevertheless, the isotopic patterns for the 8 observed signals correspond to the doubly charged $[M - 2CH_3 - nCO]^{2-}$ ions ($n$ = 2−9).

Several important pieces of structural information emerge from this observed ion-fragmentation pattern, which illustrates the mildness of the ionization process. First, the ion fragments correspond to the sequential loss of COs, which is frequently found from mass spectral analyses of fragmentation of neutral metal carbonyl clusters. Second, the presence of only $Ni_{10}Bi_2$-containing ion fragments points to the icosahedral $Ni_{10}Bi_2$ cage being intact and thereby not being inherently fragile. Third, the absence of both methyl groups in these ion fragments may be readily attributed to the

(40) Whitmire, K. H.; Shieh, M.; Cassidy, J. *Inorg. Chem.* **1989**, *28*, 3164−3170.

(41) Gavney, J. A., Jr. Ph.D. Thesis, University of Wisconsin−Madison, 1992.

(42) Longoni, G.; Heaton, B.; Chini, P. *J. Chem. Soc., Dalton Trans.* **1980**, 1537−1541.

(43) (a) Hop, C. E. C. A.; Bakhliar, R. *J. Chem. Educ.* **1996**, *73*, A162−169 and references therein. (b) Hop, C. E. C. A.; Saulys, D. A.; Gaines, D. F. *Inorg. Chem.* **1995**, *34*, 1977−1978.

(44) Arnold, L. Isotope Pattern Calculator, Ver. 1.6, 1990.

relative low binding energy of the two Bi-attached methyl substituents. In contrast, a negative-ion ESI mass spectrum of an antimony analogue, $[Ni_{10}(Sb^{i}Pr)_2(CO)_{18}]^{2-}$, displayed prominent signals that were assigned on the basis of their observed and calculated isotopic patterns to ion-fragment formulas containing Sb-attached isopropyl substituents.[19] These mass spectral differences are completely consistent with calorimetric results which showed that the bond dissociation energy of a Bi−alkyl bond is considerably smaller than that of an Sb−alkyl bond.[45] The implications of these mass spectral results are also in harmony with the unsuccessful attempts by Longoni and co-workers[20] to either protonate or methylate the Bi atoms in the $[Ni_{11}Bi_2(CO)_{18}]^{n-}$ trianion ($n = 3$) or tetraanion ($n = 4$), whereas their effort to methylate the closely related $[Ni_{11}\{SbNi(CO)_3\}_2(CO)_{18}]^{4-}$ by reaction with methyl iodide was successful in producing the $[Ni_{11}(SbMe_2)(CO)_{18}]^{2-}$ dianion containing the Ni-centered 1,12-$Ni_{10}Sb_2$ cage (*i.e.*, the Ni-centered homologue (E = Sb) of **2**).

## Experimental Section

**Methods and Materials.** All reactions including sample transfers and manipulations were carried out with standard Schlenk techniques either on a preparative vacuum line under nitrogen or within a Vacuum Atmospheres drybox under nitrogen atmosphere. The following solvents were freshly distilled under nitrogen from the indicated appropriate drying agents immediately prior to use: hexane ($CaH_2$); toluene (Na/benzophenone); tetrahydrofuran (K/benzophenone); acetone ($CaSO_4$); acetonitrile ($Na_2CO_3$); diisopropyl ether (K/benzophenone); diethyl ether (K/benzophenone).

The $[NMe_4]^+$ salt of the $[Ni_6(CO)_{12}]^{2-}$ dianion (**1**)[6] was prepared by a modification[46] of the general method of Longoni, Chini, and Cavalieri.[6b] The following materials were used without further purification: magnesium metal turnings (Fisher), carbon tetrachloride (Mallinckrodt), bismuth trichloride (Aldrich), iodomethane (Aldrich), bromine (Mallinckrodt), iodoethane (Aldrich).

Infrared spectra were obtained on a Mattson Polaris FT-IR or a Nicolet 740 FTIR spectrophotometer. Solution spectra were obtained by use of nitrogen-purged $CaF_2$ cells.

Electrochemical measurements were performed with a Bioanalytical Systems electrochemical analyzer in concert with a Princeton Applied Research electrochemical cell operating inside of a Vacuum Atmosphere drybox. The cell consisted of a glassy carbon working electrode, a platinum wire auxiliary electrode, and a standard calomel electrode (SCE). The voltage potentials were measured relative to the SCE.

**Preparation and Characterization of Alkylbismuth Dichlorides. (a) Methylbismuth Dichloride.** Magnesium turnings (4.5 g, 180 mmol), a stirbar, and 30 mL of diethyl ether were added to a two-neck 500 mL Schlenk flask equipped with a reflux condenser. Iodomethane (11.5 mL; 26.1 g, 180 mmol) dissolved in 50 mL of diethyl ether was added over 30 min to create a methyl Grignard reagent. Bismuth tribromide (25.0 g, 55.7 mmol) dissolved in 70 mL of diethyl ether was added dropwise to the methyl Grignard reagent at room temperature over another 30 min. An excess of Grignard reagent was utilized to prevent the development of partially methylated bismuth bromides. Completion of reaction was ensured by a 1-h-long reflux. By use of a distillation apparatus, both diethyl ether and trimethylbismuth were readily distilled with the receiving flask kept at −78 °C. Although suggested by Scherer,[23] distillation at high temperature and low pressure was found to be unnecessary; an unidentified orange-yellow residue sublimes at these latter conditions, but no additional trimethylbismuth was collected. The colorless distillate was fractionally redistilled (43 °C, 30 min) to remove the diethyl ether. The second fraction was a clear, colorless liquid (11.1 g) that was assumed to be a mixture of the desired product, $Me_3Bi$, and the solvent; on the basis of its measured density of 1.8 g/mL, this liquid was estimated to be about 67% pure trimethylbismuth. Yield: 56% based on $BiBr_3$.

Trimethylbismuth was slowly dripped into a solution containing 19.7 g (62.5 mmol) of bismuth trichloride dissolved in 100 mL acetone. After being stirred for 2 h, the solvent was evaporated and the residue washed several times with diethyl ether and then dried under vacuum. This procedure gave rise to 26.5 g (89.8 mmol) of methylbismuth dichloride (96% yield based on $Me_3Bi$). Methylbismuth dichloride is soluble in acetone, slightly soluble in THF, and insoluble in lower polarity solvents.

The identity of $MeBiCl_2$ was established from a mass spectrum (Kratos MS-25; resolution [5000]; electron-impact ionization, 40 eV). The sample was introduced into the ion source via a heated probe. The fragment pattern observed in the positive-ion mass spectrum includes the ion-parent peak at *m/z* 294 ($[M]^+$, 21%) and prominant ion peaks at 279 ($[BiCl_2]^+$, 70%), 259 ($[MeBiCl]^+$, 80%), 244 ($[BiCl]^+$, 45%), and 209 ($[Bi]^+$, 100%).

**(b) Ethylbismuth Dichloride.** A similar preparation of ethylbismuth dichloride was carried out. Magnesium turnings (4.5 g, 180 mmol), a stirbar, and 30 mL of ethyl ether were added to a two-neck 500 mL Schlenk flask. A reflux condenser and rubber septum were attached, and after the system was flushed with nitrogen, 14.7 mL (28.7 g, 180 mmol) of iodoethane dissolved in 30 mL of diethyl ether was added over 20 min. Bismuth tribromide (25.0 g, 55.7 mmol) dissolved in 90 mL of diethyl ether was then added over another 20 min. After the solution was refluxed for 1 h, the condenser was replaced with a distillation apparatus, and the diethyl ether was distilled off. The temperature was then raised to 140 °C, and under low pressure the reaction vessel was heated to dryness in order to distill a clear liquid into a receiving flask cooled to −78 °C. This liquid (14.5 g, 16.7 mL) was assumed to be a mixture of $Et_3Bi$ (density: 1.82 g/mL) and $Et_2O$ (0.71 g/mL); the resulting estimated yield of $Et_3Bi$ is 12.4% (2.05 g, 6.92 mmol).

This intermediate, $Et_3Bi$, was dissolved in 50 mL of acetone and slowly added to 4.4 g (13.8 mmol) of $BiCl_3$. The milky white solution quickly turned yellow; after being stirred for 2 h, the solvent was removed under a nitrogen stream. The residue was washed with diethyl ether and dried under vacuum; the resulting solid was identified as $EtBiCl_2$ (5.6 g, 18 mmol; 87% yield based on $Et_3Bi$).

**Preparation and Characterization of Icosahedral $[Ni_{10}(BiR)_2(CO)_{18}]^{2-}$ Clusters as $[NMe_4]^+$ Salts. (a) $[Ni_{10}(BiMe)_2(CO)_{18}]^{2-}$ Dianion (2).** Methylbismuth dichloride (145 mg, 0.49 mmol) and 359 mg (0.42 mmol) of $[NMe_4]_2[Ni_6(CO)_{12}]$ were placed into a 250 mL Schlenk flask as a solid mixture. After this mixture was stirred and sonicated to ensure homogeneity of mixing and then cooled to −78 °C, *ca.* 50 mL of similarly cooled THF was added via hypodermic tubing. After the mixture was stirred for 3 h, the temperature was increased to 0 °C, and the solvent and the $Ni(CO)_4$ byproduct formed were removed. Addition of hexane and then toluene to the residue gave no soluble species. Most of the residue was found to be soluble in THF; this brown extract (160 mg) primarily contained $[NMe_4]_2[Ni_{10}(BiMe)_2(CO)_{18}]$. In addition to some insoluble powder, the only other substance detected to be present was a small amount of acetone-soluble solid, identified as the unreacted nickel reagent. An estimated yield of *ca.* 45% is based upon the following assumed reaction:

$$2[\mathbf{1}] + 2MeBiCl_2 \rightarrow [\mathbf{2}] + Ni(CO)_4 + NiCl_2 + 2Cl^- + 2CO$$

The desired dianion (**2**) as the $[NMe_4]^+$ salt was crystallized from acetone/$Et_2O$ or THF/$Et_2O$ layering mixtures.

(45) Doak, G. O.; Freeman, L. D. *Organometallics Compounds of Arsenic, Antimony, and Bismuth*; Wiley-Interscience: New York, 1970; pp 1−16.

(46) Ceriotti, A.; Longoni, G.; Piva, G. *Inorg. Synth.* **1989**, *26*, 312−315.

The stoichiometry of this compound, established unambiguously from the X-ray diffraction study, was confirmed from an elemental analysis (Desert Analytics, Tucson, AZ). Calcd for $C_{28}H_{30}Bi_2N_2Ni_{10}O_{18}$: C, 19.93; H, 1.79; Bi, 24.77; N, 1.66; Ni, 34.79. Found: C, 20.18; H, 1.61; Bi, 24.51; N, 1.76; Ni, 34.53. An infrared spectrum of **2** in THF exhibited bands at 2009 (s) and 1828 (m) $cm^{-1}$. A magnetic susceptibility measurement (TME balance) at room temperature unequivocally showed a powdered sample of **2** as the $[NMe_4]^+$ salt to be diamagnetic. CV measurements of recrystallized samples of $[NM_4]_2$[**2**] in acetonitrile solution showed an irreversible oxidation at *ca.* +0.70 V.

About 0.7 mL of purified acetone-$d_6$ was saturated with selected crystals of the freshly recrystallized $[NMe_4]_2$[**2**] and diluted to 1.0 mL in a 5 mm NMR tube, which was then flame-sealed under vacuum. $^{13}C\{^1H\}$ NMR spectra were obtained under the following conditions: the Brucker AM-500 instrument was operated at 125.7 MHz synthesizer frequency, 5.0 $\mu$s pulse width, repetition time of 0.42 s, for tens of thousands pulses at 223 K. The downfield acetone peak at 206.00 ppm was used as an internal standard.[42] The spectrum showed peaks at $\delta$ −8.67 (Bi−$\underline{C}H_3$), 54.31 ($J$ = 7.0 Hz, N($\underline{C}H_3)_4^+$), 193.83 (terminal $\underline{C}O$), 249.38 ppm (bridging $\underline{C}O$). A $^1H$ spectrum of $[NMe_4]_2$[**2**] at room temperature showed signals at $\delta$ 2.37 (s, 6H, Bi−$CH_3$) and 3.46 ppm (t, 24H, N$(CH_3)_4$, $^2J(^1H-^{15}N)$ = 0.61 Hz).

Mass spectra of $[NMe_4]_2$[**2**] were obtained with a VG AutoSpecE triple-sector (EBE) mass spectrometer (mass range 200−4000) equipped with the Mark II electrospray ionization (ESI) source and operated in the negative-ion mode with an accelerating voltage of 4000 eV. The ESI source has larger orifices for the skimmer cones, increased pumping capacity, and a hexapole focusing unit to improve sensitivity and ease of use. Experiments were carried out with a resolution of 2000 and a scan speed of 4.0 s per decade. Nitrogen was used as both the nebulizer gas (16 L/h) and the bath gas. $[NMe_4]_2$[**2**] was dissolved in acetonitrile (*ca.* $10^{-5}$ M), and the flow rate was approximately 15 $\mu$L/min. The following prominent centered doubly charged ion-fragment signals were obtained: *m/z* 725.9 ($[Ni_{10}Bi_2(CO)_{16}]^{2-}$, 3%), 711.9 ($[Ni_{10}Bi_2(CO)_{15}]^{2-}$, 7%), 697.8 ($[Ni_{10}Bi_2(CO)_{14}]^{2-}$, 5%), 683.8 ($[Ni_{10}Bi_2(CO)_{13}]^{2-}$, 42%), 669.9 ($[Ni_{10}Bi_2(CO)_{12}]^{2-}$, 100%), 655.9 ($[Ni_{10}Bi_2(CO)_{11}]^{2-}$, 37%), 639.9 ($[Ni_{10}Bi_2(CO)_{10}]^{2-}$, 31%), 627.8 ($[Ni_{10}Bi_2(CO)_9]^{2-}$, 15%). Each of these centered ion signals consists of an observed isotopic pattern that is consistent with the calculated pattern based on the assigned ion-fragment formula. For example, the observed relative values of the middle 11 isotopic mass components in the isotopic pattern for the signal centered at *m/z* 670 are 42:11:76:19:100:25:96:25:72:20:42; these values are completely consistent with those simulated[44] for the isotopic mass distribution in the $[Ni_{10}Bi_2(CO)_{12}]^{2-}$ ion fragment, *viz.*, 43:8:81:17:100:24:92:24:68:19:42. The other observed and calculated isotopic patterns of each signal also have a similar alternation of strong and weak isotopic mass components due to each ion fragment containing the intact icosahedral $Ni_{10}Bi_2$ cage and to nickel having three abundant even mass number isotopes (*i.e.*, the five naturally occurring nickel isotopes are as follows: $^{58}$Ni, 68.1%; $^{60}$Ni, 26.2%; $^{61}$Ni, 1.1%; $^{62}$Ni, 3.6%; $^{64}$Ni, 0.9%) and bismuth consisting of only one nuclide (*viz.*, $^{209}$Bi, 100%).

The possibility that the observed isotopic pattern of each doubly charged ion-fragment signal may be due to a mixture of corresponding $[Ni_{10}Bi_2(CO)_x]^{2-}$ and $[Ni_{10}(BiMe)_2(CO)_{x-1}]^{2-}$ ion fragments ($x$ = 9−16) was investigated. Because the two masses of each pair of the corresponding two ion fragments (*i.e.*, with the same $x$ value) are only 2 Da apart, and thus the two ion fragments would display overlapping isotopic patterns, a detailed analysis of the observed isotopic pattern for each signal with simulated isotopic patterns for each of the two pure ion fragments and for mixtures of the corresponding $[Ni_{10}Bi_2(CO)_x]^{2-}$ and $[Ni_{10}(BiMe)_2(CO)_{x-1}]^{2-}$ ion fragments was carried out. Because in each case the observed isotopic pattern closely matches the calculated pattern for either of the two pure fragments and not a mixture, and because in each case the signal matches that for the pure nonmethylated $[Ni_{10}Bi_2(CO)_x]^{2-}$ ion fragment and not that for the corresponding Bi-methylated one, we conclude that it is highly unlikely that any of the 8 centered signals results from inclusion of the corresponding Bi-methylated $[Ni_{10}(BiMe)_2(CO)_{x-1}]^{2-}$ ion fragment.

**(b) $[Ni_{10}(BiEt)_2(CO)_{18}]^{2-}$ Dianion (3).** Ethylbismuth dichloride (140 mg, 0.49 mmol) and 360 mg (0.43 mmol) of $[NMe_4]_2[Ni_6(CO)_{12}]$ were placed as a solid mixture into a 250 mL Schlenk flask. After this mixture was briefly sonicated to ensure homogeneity of mixing and then cooled to −78 °C, approximately 50 mL of similarly cooled THF was added via hypodermic tubing. After the solution was stirred for 3 h, the temperature was increased to 0 °C, and the solvent was removed. No soluble hexane or toluene species were obtained via sequential extractions of the residue with these solvents. The brown THF extract gave the major product of this reaction which was identified as $[NMe_4]_2[Ni_{10}(BiEt)_2(CO)_{18}]^{2-}$. Beside a copious amount of insoluble material, the only other isolated material consisted of a small amount of acetone-soluble solid, which was identified as the unreacted $[NMe_4]^+$ salt of **1**. The $[NMe_4]^+$ salt of **3** did not crystallize as easily as that of the methylbismuthinidene **2**.

An infrared spectrum of **3** in THF displayed maxima at 2005 (s) and 1830 (m) $cm^{-1}$.

**X-ray Crystallographic Determinations and Refinements. (a) General Procedures.** Each crystal was mounted under an argon atmosphere either onto a thin glass fiber and coated with epoxy or inside of a Lindemann glass capillary which was then hermetically sealed. Intensity data were obtained with graphite-monochromated Mo K$\alpha$ radiation on a Siemens P4 diffractometer[47] equipped with a sealed tube generator. Intensities of standard reflections showed no significant variations during the entire collection of data. Empirical absorption corrections based upon $\psi$-scan measurements at different azimuthal angles were applied to each data set. Crystallographic computations were carried out with SHELXTL PLUS run on a Silicon Graphics Indy work station.[48] Preliminary positions of the heavy atoms were found by direct methods, while positions of the other non-hydrogen atoms were determined from successsive Fourier difference maps coupled with initial isotropic least squares.[49] Final Fourier difference maps exhibited no unusual features for each structure. Crystal data, data-collection, and refinement parameters are presented in Table 1.

**(b) $[NMe_4]^+_2[Ni_{10}(BiMe)_2(CO)_{18}]^{2-}$ Dianion (2).** Crystals of this compound were obtained by various methods, including the layering of low-polarity solvents such as hexane, diethyl ether, or diisopropyl ether over high-polarity solutions (such as THF or acetone) containing the dissolved product. X-ray data were obtained at −140 °C from a block-shaped crystal, isolated from an acetone/diisopropyl ether solution, which was found to be monoclinic. X-ray data were initially collected with a Siemens P4 diffractometer, from which the crystal structure was determined and refined ($R_1(F)$ = 0.11). Subsequently, better crystals were grown, and X-ray data were obtained with a Siemens P4/CCD diffractometer; the resulting refinement gave much better crystallographic results. Figure 1 shows the configuration of the dianion and its $Ni_{10}Bi_2$ icosahedral cage in the $[NMe_4]^+$ salt.

**(c) $[NMe_4]^+_2[Ni_{10}(BiEt)_2(CO)_{18}]^{2-}$ Dianion (3).** Crystals of this compound were obtained by the layering of hexane over

(47) Data Collection: SMART Software Reference Manual (1994). Siemens Analytical X-ray Instruments, 6300 Enterprise Dr., Madison, WI 53719−1173.

(48) Data Reduction: SAINT Version 4 Software Reference Manual (1995). Siemens Analytical X-ray Instruments, 6300 Enterprise Dr., Madison, WI 53719−1173.

(49) Structure Solution, Refinement and Graphics: Sheldrick, G. M. SHELXTL Version 5 Reference Manual (1994). Siemens Analytical X-ray Instruments, 6300 Enterprise Dr., Madison, WI 53719−1173. Neutral atom scattering factors were taken from: *International Tables for Crystallography*; Kluwer: Boston, MA, 1995; Vol. C, Tables 6.1.1.4 and 4.2.6.8.

a THF solution containing the dissolved product to give block-shaped crystals or by vapor diffusion of acetone solution with diisopropyl ether solvent to give needle-shaped crystals. X-ray data were collected at −125 °C from a parallelepiped crystal, which was found to be triclinic. A statistical analysis of the data indicated that the probable space group to be $P\bar{1}$. Figure 2 shows the configuration of the dianion in the $[NMe_4]^+$ salt.

**Acknowledgment.** The authors thank the National Science Foundation (Grants CHE-9013059 and CHE-9310428) for support of this research. Departmental purchase of the Siemens P4/CCD area detector diffractometry system and associated computer equipment utilized in this research was made possible by funds from the NSF (Grants CHE-9105497 and CHE-9310428) and the Graduate School of UW−Madison. Additionally, we are greatly indebted to Dr. Marcel Hop (Chem. Dept., UW−Madison) for the ESI mass spectrometric measurements, to David Snyder (Chem. Dept., UW−Madison) for the EI mass spectrometric measurements, to Professor Charles P. Gibson (Chem. Dept., UW−Oshkosh) for the magnetic susceptibility measurements, and to Dr. Randy K. Hayashi and Dr. Douglas R. Powell (Chem. Dept., UW−Madison) for crystallographic assistance.

**Supporting Information Available:** Crystallographic tables for the $[NMe_4]^+$ salts of $[Ni_{10}(BiMe)_2(CO)_{18}]^{2-}$ (**2**) and $[Ni_{10}(BiEt)_2(CO)_{18}]^{2-}$ (**3**) listing atomic coordinates, anisotropic thermal displacement parameters, interatomic distances, bond angles, and idealized hydrogen coordinates (12 pages). Ordering information is given on any current masthead page.

OM960965K